Contents lists available at ScienceDirect

Journal of Contaminant Hydrology

journal homepage: http://ees.elsevier.com

Geochemical evolution and tracing of groundwater salinization using different ionic ratios, multivariate statistical and geochemical modeling approaches in a typical semi-arid basin

Emmanuel Daanoba Sunkari [a,b,*], Mahamuda Abu [c], Musah Saeed Zango [c]

[a] Department of Geological Engineering, Faculty of Engineering, Niğde Ömer Halisdemir University, Main Campus, 51240 Niğde, Turkey
[b] Department of Geological Engineering, Faculty of Mineral Resources Technology, University of Mines and Technology, P.O. Box 237, Tarkwa, Ghana
[c] Department of Earth Science, Faculty of Earth and Environmental Sciences, CK Tedam University of Technology and Applied Sciences, P.O. Box 24, Navrongo, Ghana

ARTICLE INFO

Keywords
Groundwater chemistry
Groundwater salinization
Ionic ratio plots
Multivariate statistical analyses
Geochemical modeling
Semi-arid Pru Basin

ABSTRACT

The vulnerability of semi-arid basin aquifers to long-term salinization due to the dissolution of groundwater chemical constituents is a major global problem. Despite this, resilient techniques of tracing the sources of groundwater salinization in semi-arid basin aquifers are still evolving due to the aquifer complexities. This study proves the effectiveness of the use of different ionic ratios, multivariate statistical, and geochemical modeling approaches to understand groundwater evolution and trace salinization in the semi-arid Pru Basin of Ghana. The basin is homogeneously composed of argillaceous sediments of the Oti/Pendjari Group of the Voltaian Supergroup. A total of 81 samples from hand-dug wells and boreholes within the Pru Formation of the Oti/Pendjari Group in the basin were collected for this study. Quantitative analysis of the data shows that the abundance of major ions follows the order: $Na^+ > Ca^{2+} > Mg^{2+} > K^+$ and $Cl^- > HCO_3^- > SO_4^{2-}$. The groundwater evolved from Na-HCO3, Na-HCO3-Cl, Na-Ca-HCO3 to Na-Mg-HCO3 water types in a decreasing order of abundance. Calculated meteoric genesis index (r2) indicates the dominance of deep meteoric water percolation effects on groundwater chemistry. Groundwater chemistry is principally controlled by water-rock interaction, ion exchange reactions, weathering (carbonate and silicate), salinization, and anthropogenic activities. Different ionic ratio plots and spatial distribution maps reveal the prevalence of salinization in the aquifer system, especially around the southwestern part of the basin. Revelle index assessment of the groundwater salinization level indicates that about 19.8% of the groundwater samples with RI values >0.5 is influenced by salinization. The groundwater salinization results from saline water intrusion from adjacent aquifers, mixing effects, ion exchange reactions, water-rock interaction, and anthropogenic activities. The geochemical modeling involving thermodynamic calculation of mineral saturation indices in PHREEQC indicates that groundwater is largely saturated with respect to majority of the carbonate and silicate mineral phases.

1. Introduction

The demand for groundwater for various purposes, starting from the home to the industry keeps increasing owing to the increasing global population. The hike in global population has also led to urbanization, industrialization, increasing commercial agricultural activities, and demand for food, which make it important to continuously assess the chemical quality of groundwater (Sunkari et al., 2020). Although the demand for quality groundwater to support the ever growing global population is on the rise, the aforementioned activities, which are equally necessary for a sustainable growing population have adverse effects on the quality of groundwater available for domestic, agricultural and industrial usage (Yidana et al., 2018; Sunkari et al., 2019, 2020). The safe usage of groundwater for agricultural, domestic and industrial purposes depends on the chemistry of the groundwater (Rufino et al., 2019). It is widely known that the chemistry of groundwater is controlled by several geogenic factors including precipitation composition, weathering, geology and mineralogy of aquifers, and geochemical processes occurring in aquifers (Belkhiri et al., 2012; Sunkari et al., 2018; Kaur et al., 2019; Karunanidhi et al., 2020). Interaction among all these factors results in various hydrochemical facies or water types. These hydrochemical facies are mostly determined from major ion studies and their spatial variability usually gives vital information on aquifer characteristics (Belkhiri et al., 2012; Busico et al., 2018). Among the geogenic factors that control groundwater chemistry, weathering of the rocks through which

* Corresponding author at: Department of Geological Engineering, Faculty of Engineering, Niğde Ömer Halisdemir University, Main Campus, 51240 Niğde, Turkey.
E-mail address: emmanueldaanoba.sunkari@mail.ohu.edu.tr (E.D. Sunkari)

https://doi.org/10.1016/j.jconhyd.2020.103742
Received 10 August 2020; Received in revised form 12 November 2020; Accepted 17 November 2020
Available online xxx
0169-7722/

groundwater is transmitted and ion exchange reactions play a critical role. The weathering rate of rocks and ion exchange reactions are controlled by groundwater residence time, pH and temperature (Yidana et al., 2012). A classic example is the dissolution rate of crystalline rocks and the silicate minerals they contain, which involves a very slow process that is enhanced by low pH and high temperatures (Chegbeleh et al., 2020).

Moreover, anthropogenic activities such as mining, agriculture, unplanned developments and other human activities have been documented as sources of groundwater pollution (e.g., Lermi and Ertan, 2019; Sunkari et al., 2019; Zango et al., 2019; Abanyie et al., 2020; Gibrilla et al., 2020). Through these activities, heavy metals and pesticides have the proclivity of seeping into aquifers and thus, influencing the chemistry of groundwater, ultimately leading to groundwater pollution. For instance, Sunkari and Abu (2019) studied the sources of groundwater fluoride in the Bongo district of the Upper East Region of Ghana using hydrochemical and multivariate statistical approaches. They suggested that in addition to the geogenic origin of the groundwater fluoride, anthropogenic sources such as the use of phosphate fertilizers also contributed greatly to the fluoride loading in the groundwater. Anthropogenic pollution of groundwater mostly occurs in shallow unconfined aquifers than deep confined aquifers. This is because the shallow unconfined aquifers typically occur a few meters beneath the subsurface and are therefore liable to pollution by surficial contaminant sources. Therefore, areas that have unprotected recharge zones and unregulated surface activities are likely to be hit hard by groundwater pollution.

One of the major global threats to groundwater quality in coastal and basinal areas is salinization. Groundwater salinization comes from different sources including seawater intrusion (Pratheepa et al., 2015; Najib et al., 2017; Egbi et al., 2019), ion exchange reactions (Pratheepa et al., 2015), dissolution of secondary minerals (Ammar et al., 2020), saline water flow from adjacent aquifers (Egbi et al., 2019), return flow from irrigation water (Kass et al., 2005), evapotranspiration (Cartwright and Morgenstern, 2012), anthropogenic input (Karunanidhi et al., 2020), climate change and land use (Borrok and Engle, 2014) or commonly, a combination of most of these sources (Keesari and Dauji, 2020). Groundwater salinization is harmful to cropping soils as it causes accumulation of higher amounts of salt that affects salt-intolerable crops. This calls for the need to characterize and identify groundwater salinization processes in coastal and basinal areas for sustainable management of groundwater resources.

As a strategic way of protecting groundwater resources, geoscientists now focus more on understanding the geochemical evolution of groundwater using multivariate statistical techniques such as factor analysis and principal component analysis (Belkhiri et al., 2010, 2012; Yidana et al., 2012, 2018; Loh et al., 2019; Sunkari and Abu, 2019; Sunkari et al., 2019, 2020; Zango et al., 2019; Çiner et al., 2020). These approaches are able to analyze all the parameters, thus the cations and anions in a sample suite by reducing and classifying the data. They are able to extract vital information from hydrochemical datasets even in complex hydrogeological systems. Also, spatial distribution maps of hydrochemical parameters have been effectively used in delineating areas under threat of pollution (e.g., Gnanachandrasamy et al., 2015; Zango et al., 2019; Sunkari et al., 2020). Furthermore, the development of geochemical modeling in geoscience has led to the use of major ions to deduce the physico-chemical processes controlling groundwater chemistry (Belkhiri et al., 2010; Salifu et al., 2012; Zango et al., 2019; Karunanidhi et al., 2020; Lyons et al., 2020). The most common geochemical modelling approach used in hydrogeochemical studies is thermodynamic calculation of the saturation indices of mineral phases in PHREEQC (Parkhurst and Appelo, 1999). It uses geochemical parameters and computes the saturation indices of minerals that are capable of pervading a solution. Therefore, a combination of all these approaches will help in understanding the geochemical evolution of groundwater and sources of pollution in the study area.

The semi-arid Pru Basin covers most areas in the Bono East Region of Ghana, where farming and fishing are the dominant occupation. The region is widely known to be the food basket of the nation and this has resulted in the migration of farmers from the northern and the two upper regions of Ghana. As the food basket of Ghana, commercial farming in this region involves the use of weedicides/herbicides, fertilizers and other farming inputs within the semi-arid Pru Basin. This part of Ghana is characterized by a very thick regolith profile due to the prevailing climatic conditions in the area, which tends to support deeper chemical weathering. The predominance of agricultural activities in and around the semi-arid Pru Basin coupled with its thick regolith profile has the tendency of influencing the groundwater chemistry via infiltration from agricultural lands as well as disposables from the growing agrochemical shops and factories within the catchment of the basin, not precluding geogenic source effect. Eventually, the quality of the water would be affected, which can greatly impact the health and livelihood of the rural dwellers. Moreover, all the rivers in the semi-arid Pru Basin form part of the Volta River drainage system serving as tributaries to the Volta Lake. In the wake of these potential threats to the groundwater quality in the area, there is little data available on the current nature of groundwater chemistry in the area and hence, the quality to allow for monitoring and designing of proper management practices within the catchment of the semi-arid Pru Basin is not well documented in the literature. The mechanisms responsible for groundwater chemistry in the semi-arid Pru Basin are still not properly understood. Therefore, the primary objectives of this study are to assess the geochemical composition of groundwater and to determine geogenic and anthropogenic controls of groundwater chemistry in the semi-arid Pru Basin using ionic ratio plots, multivariate statistical and geochemical modeling approaches. The research will contribute to the understanding of the vulnerability of basinal aquifers to long-term salinization in a broad context through the dissolution of groundwater chemical constituents. The use of different ionic ratio plots and geochemical modeling to depict groundwater salinization is still not common in the scientific front. Most studies employ single ionic plots such as (Na^+/Cl^-) versus ionic concentration of (Cl^-) to show groundwater salinization but such plots in which both axes have a common variable (Cl^-) can reveal trends that may be totally unrelated to hydrogeochemical processes and thus, may be induced resulting in 'common variable effect on correlation' or 'spurious correlation' (Keesari and Dauji, 2020). As a result, it is better to always use different ionic ratio plots involving Na^+, K^+, Ca^{2+}, Mg^{2+}, Cl^-, SO_4^{2-} and B alongside mineral saturation indices to verify groundwater salinization as done in this study. In all, this study is the first to document evidence of groundwater salinization in the semi-arid Pru Basin. The results of this study will guide policy-makers and stake-holders in designing effective ways of protecting groundwater resources in the area. The recommendations made can be extrapolated to similar areas in the world.

2. Study area

2.1. Location, climate and drainage features

The semi-arid Pru Basin covers the area between longitudes 00°45′ to 01°15′ W and latitudes 07°45′ to 08°15′ N (Fig. 1a). It lies in the central part of the Bono East Region of Ghana with a small area between Prang and Abease as part of the Northern Region of Ghana. The area lies in the southern part of the so-called 'Middle Belt' of Ghana and is located along the main route between Ejura and Salaga. The area is situated in the central domain of Ghana and is partially bounded by the Volta Lake in the east. It is characterized by periods of wetness and dryness. March–July is the major rainy season, with June as the wettest

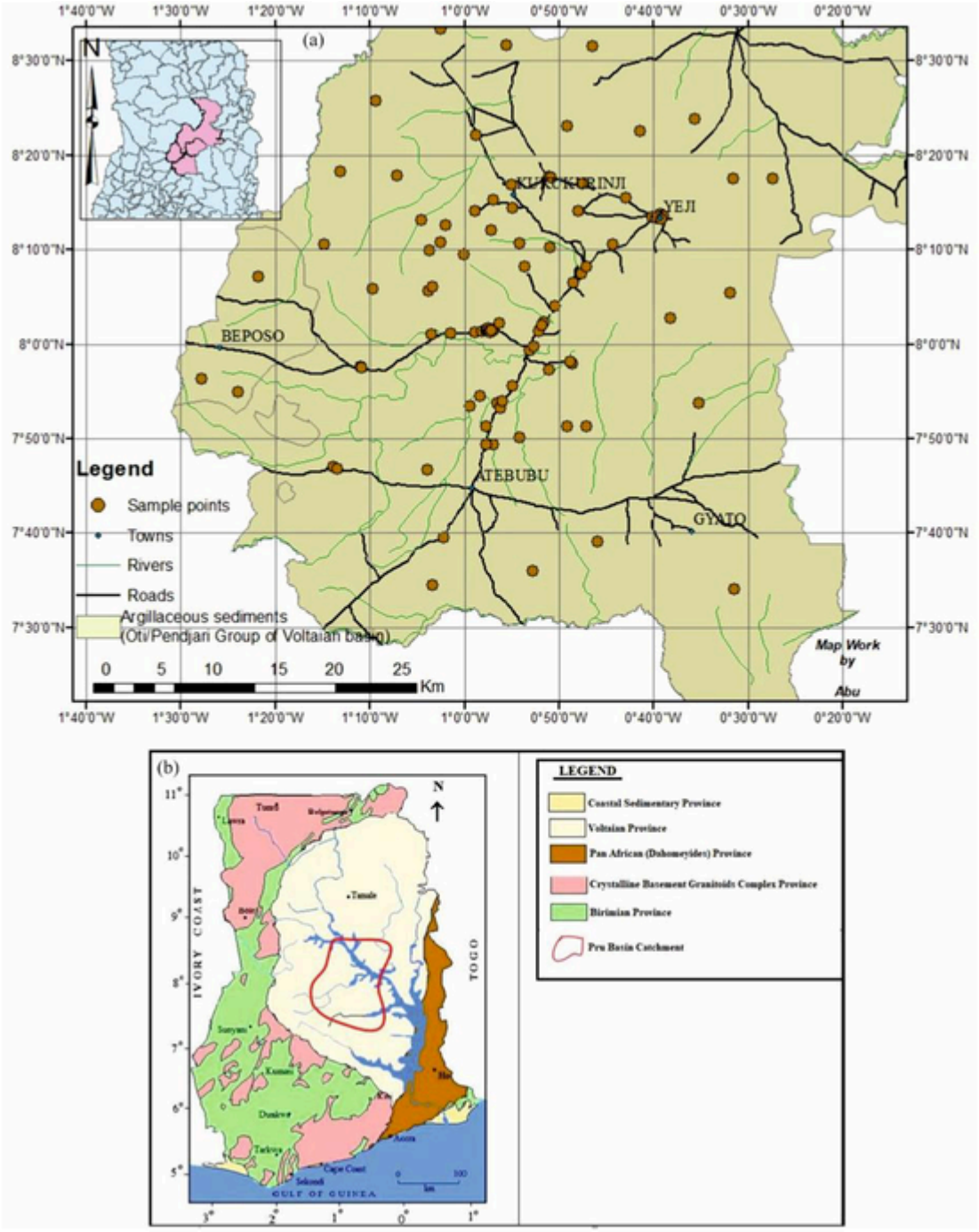

Fig. 1. (a) Location and geology map of the semi-arid Pru Basin showing the sampling points and (b) hydrogeological map of Ghana with the semi-arid Pru Basin in perspective.

month, whereas November–February is the major dry season. August is the shortest or minor dry season time, and September–October is the shortest rainy season. Mean rainfall is about 1150–1250 mm (lowest about 330 mm and highest about 1500 mm). The highest temperatures (mean shade maximum approximately 30 °C) occur just before the rainy season and the lowest (mean shade minimum about 24 °C) occur during the peak wet months (Junner and Hirdes, 1946). Almost all the rivers in the area form part of the Volta River drainage system. The most important is the Pru River of which, the majority of the rivers are its tributaries. The Pru River flows from the southwest to the northeast, where it enters the Volta Lake.

2.2. Geology and hydrogeology

The semi-arid Pru Basin forms part of the Neoproterozoic to Paleozoic flat-lying sedimentary succession of Ghana known as the Voltaian Supergroup. The Voltaian Supergroup is composed of three main groups, from top to bottom as Tamale/Obosum Group, Oti/Pendjari Group and Kwahu/Bombouaka Group (Abu et al., 2019). The semi-arid Pru Basin is entirely overlain by the Oti/Pendjari Group (Fig. 1a) with outcrops mainly in the eastern and northern fringes. The Pru Formation within this group consists mainly of reddish-brown, interbedded mudstone and sandstone (Affaton, 2008). The basal part of the unit is

more sandstone-rich, becoming richer in mudstone higher up, to the north and east of Prang (Carney et al., 2008). Ferricrete covers most of the area and is absent only along the main rivers. Small scarps are sometimes formed at where the rivers cut through the ferricrete. The ferricrete occurs below a variable thickness of soil overlying the bedrock. The ferricrete is up to 1.5 m thick, locally thicker. It usually contains angular fragments of the underlying mudstone and sandstone. These fragments lack any indication of transportation and are from local geological formations. In situ ferricretization of the underlying sediments is evident. No deep weathering of bedrock below the ferricrete can be observed. Numerous wells, usually about 0.5 m in diameter, have been dug through the ferricrete and the underlying mudstone, and hollowed out to depths of 3–4 m to store rainwater.

The semi-arid Pru Basin forms a significant portion of the Voltaian hydrogeological province in Ghana, which is coterminous with the Volta Lake (Fig. 1b). It is characterized by altering argillaceous and arenaceous rocks and the wide-spread presence of ferricretes (Griffis et al., 2002), which significantly affect the depth of weathering and restrict recharge. Therefore, aquifers are shallow and fractured, with deep weathering being restricted by the ferricrete. The lithology and jointing of the bedrock below the ferricrete is expected to affect permeability. In general, the aquifer is semi-confined by the ferricrete, and the water level follows the topography. Borehole depths range between 45 and 75 m and aquifers are generally encountered between the depth range of 20 and 30 m. The success rate of drilling boreholes in the Pru Formation is about 50% and it is among the lowest in the country. Primary porosities are very low owing to the impervious nature of the rocks but are enhanced by fracturing and weathering. Therefore, the hydrogeological parameters are primarily based on secondary structures in the form of joints developed after the primary porosities had been destroyed in the wake of rock compaction and slight metamorphism. This has resulted in a wide range of hydrogeological properties. The hydrogeological properties of the study area are not favourable for large-scale groundwater development since yields are generally less than 3.5 m^3/h (Dapaah-Siakwan and Gyau-Boakye, 2000). However, yields as high as 15 m^3/h are occasionally encountered. The depth of the weathered zone provides potential for increased groundwater storage, however, the low permeability limits abstraction. The depths of aquifers are normally between 20 and 60 m with alluvial deposits defining most of the main river channels (Sikah et al., 2016). They are generally fine-grain deposits, mainly silty and clayey, hence, they form poor aquifers. Groundwater quality issues related to elevated nitrates exist in some communities owing to localized pollution from agricultural activities around open shallow wells.

3. Methodology

3.1. Data collection and analysis

A total of 81 samples were collected from 70 hand-dug wells and 11 boreholes using 300 mL plastic bottles. The samples from the hand-dug wells were collected using a Klyen downhole stainless steel borehole sampler whereas the samples from the boreholes were collected by direct pumping from the installed pumps of the boreholes. At each of the sampling points, the 300 ml plastic bottles were rinsed with the water to be collected to reduce or completely eliminate any contaminations that might be introduced and then filled to the brim. Geo-satellite positioning of all the 81 sampling points were determined with a GPS device. The collected samples were immediately stored in ice-chests containing ice cubes to prevent reactions within the water. The samples were then taken to the Ghana Atomic Energy Commission in Accra for geochemical analysis. Physico-chemical parameters such as pH, temperature, total dissolved solids (TDS), and electrical conductivity (EC) were measured directly in the field from the hand-dug wells and boreholes using WTW ProfiLine 3320 Universal Multi-parameter Portable Meter. Major ions such as potassium (K^+) and sodium (Na^+) were analyzed using flame photometer. Magnesium (Mg^{2+}) and calcium (Ca^{2+}) concentrations were determined using the AA240FS Fast Sequential Atomic Absorption Spectrometer. ICS-90 Ion Chromatograph (DIONEX ICS-90) was used in determining carbonate (CO_3^{2-}), bicarbonate (HCO_3^-), chloride (Cl^-), fluoride (F^-), nitrate (NO_3^-), and sulfate (SO_4^{2-}) concentrations. Boron (B) concentrations were analyzed using fluorescence analyzer. The detection limits for all the ions were K^+ (0.1 mg/L), Na^+ (0.01 mg/L), Mg^{2+} (0.05 mg/L), Ca^{2+} (0.05 mg/L), CO_3^{2-} (0.03 mg/L), HCO_3^- (0.03 mg/L), Cl^- (0.2 mg/L), F^- (0.02 mg/L), NO_3^- (0.05 mg/L), SO_4^{2-} (0.1 mg/L), and B (0.005 mg/L). In order to maintain the accuracy and a degree of confidence in the integrity of the data, all the sampling bottles and glassware were soaked in a 5% nitric acid for overnight and rinsed with deionized water before use. Instruments used were calibrated with standard chemical solutions prepared from commercially available chemicals and validated with Standard Reference Materials (SRM) and Certified Reference Materials (CRM). The SRM were analyzed repeatedly at predetermined intervals to confirm that the method remained in a state of statistical control. Duplicate samples were also measured and compared and their results were found reproducible within ±5% error limit. Again, accuracy of the laboratory analysis was checked by calculating the cation-anion balance errors and only those results with errors ±5% were relied on for subsequent interpretation.

3.2. Multivariate statistical techniques

R-mode Factor Analysis (FA) and Principal Component Analysis (PCA) were the main statistical techniques employed in this study. These techniques are used to reduce the complexity of large-scale datasets and show the relationship between data components (Sunkari et al., 2020). By using these techniques, factors with eigenvalues ≥1 were considered as a possible variance in the study. The algorithm employed for extraction of the factors was the PCA whilst Varimax rotation was the rotation criterion. The multivariate statistical analyses were done using SPSS Statistics version 25. However, ionic ratios (bivariate plots) were plotted for pairs of related chemical species using AquaChem version 4.0. The ratios between major ions were employed to determine the variable dependency and the relationships between a variable pair in the water.

3.3. Hydrochemical graphing and geochemical modeling

In this study, AquaChem version 4.0 was used in producing Piper and Gibbs plots to identify the hydrochemical facies and the mechanisms controlling the groundwater chemistry. Spatial distribution maps of the hydrochemical parameters were produced by means of Surfer version 11 using kriging interpolation. Kriging was the preferred interpolation technique because it addresses surface estimation problems by using semi-variograms (Sunkari and Abu, 2019). PHREEQC (Parkhurst and Appelo, 1999) was employed in performing thermodynamic calculation of the saturation indices (SI) of the various mineral phases residing in the groundwater using eq. 1.

$$SI = \text{Log } (IAP/K_{sp}) \quad (1)$$

where IAP stands for the ion activity of the solution and K*sp* is the solubility constant at a particular temperature. In the current study, carbonate and silicate minerals were the most important during the thermodynamic calculation of the saturation indices since the aquifer materials in the study area are dominated by carbonate rocks and silicate minerals. SI less than zero is an indication that the groundwater is under-saturated with respect to the particular mineral and such value is a reflection of the nature of the groundwater in an environment of formation, which contains less amount of the mineral in solution. It also

points to shorter residence times of the groundwater (Ako et al., 2012). SI value greater than zero suggests that the groundwater is supersaturated with respect to the given mineral in solution and the water is unable to further dissolve the mineral.

3.4. Groundwater salinization

Revelle index was used in assessing the level of groundwater salinization in the study area. The Revelle Index was computed from the equation below.

$$\text{Revelle index (RI)} = Cl^{-} / \left(HCO_3^{-} + CO_3^{2-}\right) \quad (2)$$

The concentrations of the ions used in the above equation are expressed in meq/L. According to Karunanidhi et al. (2020), groundwater with RI values >0.5 is said to be influenced by salinization. After identifying the level of groundwater salinization using the RI approach, ionic ratio plots were produced to identify the sources of the salinization.

4. Results

4.1. Geochemical characterization

The physico-chemical parameters of the samples were evaluated with reference to guidelines for drinking water provided by the World Health Organization (World Health Organization, W.H.O, 2017). They are presented in Table 1 and summarized in Table 2. The pH levels of majority of the samples are within the WHO acceptable limits (6.5–8.5) and closely vary between 7.77 and 8.63 with an average value of 8.29. However, 8 samples (2 boreholes and 6 hand-dug wells) have higher pH values when compared to the acceptable limits. The high pH values in these boreholes and hand-dug wells is attributed to the dominance of limestone in the communities where they are located (Fig. 1a). This is because, limestone contains carbonate, bicarbonate and hydroxide compounds that are capable of dissolving and mixing with the water, raising the pH level of the water. The samples have widely varied electrical conductivity (EC) values in the range of 306–7914 μS/cm with an average value of 797 μS/cm, which suggests noncompliance with the World Health Organization, W.H.O (2017) guideline value of 2500 μS/cm. The measured isolated cases of very high EC values of 7914 μS/cm and 2604 μS/cm in hand-dug well samples PJ009 (Adeemra community) and PJ020 (Burkina Bumbo community), respectively (Table 1) are due to longer residence time of the groundwater in the aquifer. Works conducted in some parts of the Volta Basin of Ghana, which serves as the main reservoir for the semi-arid Pru Basin reported very high EC values in groundwater. For instance, Egbi et al. (2019) and Tay (2012) reported 141–19,370 μS/cm and 147–23,200 μS/cm at the lower and middle parts of the Volta Basin, respectively. Though these areas are not specifically in the current study area, the high EC values indicate that some form of mixing of freshwater and saline water may have occurred as suggested by Egbi et al. (2019). Total dissolved solids (TDS) concentrations vary between 275 and 7123 mg/L with an average value of 717 mg/L, exceeding the World Health Organization, W.H.O (2017) guideline value of 500 mg/L. The TDS values in the study area can be compared with those (70–9680 mg/L, mean of 1237 mg/L) reported from the Lower Volta River Basin (Egbi et al., 2019) and those (62–11,900 mg/L) reported from the Middle Volta River Basin (Tay, 2012). More so, the geology of the Middle Volta River Basin in the study of Tay (2012) overlaps with the geology of the semi-arid Pru Basin as they are both dominated by rocks belonging to the Oti/Pendjari Group. In this regard, the high TDS values imply high amount of charged species and longer water-rock interaction within the aquifer system (Sunkari et al., 2019). The abundance of feldspars and quartzitic sandstones in the Oti/Pendjari Group in the study area (Fig. 1a) may also account for the high TDS values. Moreover, anthropogenic activities largely as run-offs and infiltration from farm lands in the semi-arid Pru Basin cannot be precluded from influencing the TDS concentrations in the groundwater as there is a very strong positive correlation (r = 0.99) between TDS and chloride (Cl^{-}) (Table 3).

Among the major ions, only sodium (Na^{+}) concentrations exceeded the maximum permissible limit (200 mg/L) of the WHO. The Na^{+} concentrations varied from 25.2 to 2115 mg/L with an average value of 226 mg/L. A total of 26 samples (4 boreholes and 22 hand-dug wells) representing about 32.1% of the total samples have Na^{+} concentrations exceeding the guideline value. The high Na^{+} concentrations are likely due to ion exchange reactions in the aquifer (Yidana et al., 2018). There is a very strong to moderate correlation between Na^{+} and Ca^{2+} (r = 0.89), Na^{+} and Cl^{-} (r = 0.97), Ca^{2+} and Cl^{-} (r = 0.94), K^{+} and Cl^{-} (r = 0.54), and Na^{+} and K^{+} (r = 0.52) (Table 3). All these open a window of interpretation for a common geochemical source of the ions, likely salinization via ion exchange reactions (Gopinath et al., 2014). The concentrations of K^{+}, Ca^{2+}, and Mg^{2+} in the studied samples fall within the guideline values except one sample (PJ009 – Adeemra community), which has Ca^{2+} concentration of 505 mg/L exceeding the maximum permissible value of 200 mg/L (Table 1).

Cl^{-} has the highest concentration among the anions ranging from 1.36 to 4671 mg/L and an average concentration of 240 mg/L. A total of 11 hand-dug wells have very high Cl^{-} concentrations when compared with the WHO (2017) maximum permissible limit of 250 mg/L. Ion exchange reactions in the aquifer system may be responsible for the high Cl^{-} concentrations, consistent with the high TDS and EC values. Bicarbonate (HCO_3^{-}) is the most dominant anion with concentrations in the range of 121–641 mg/L and an average value of 430 mg/L. The HCO_3^{-} concentrations may be controlled by reaction of carbon dioxide in the atmosphere and soil that produces carbonic acid in the soil (Loh et al., 2019), which chemically disintegrates feldspars in the sandstones of the Oti/Pendjari Group during infiltration. The fluoride (F^{-}) concentrations are in the range of 0.23 and 3.40 mg/L with an average of 0.70 mg/L. Hand-dug wells in Parambo No. 1, Burkina Bumbo and Wurukasa communities have slightly elevated F^{-} concentrations of 2.70 mg/L, 2.23 mg/L and 3.40 mg/L, respectively. The high F^{-} in these areas is due to ion exchange reactions in the aquifer considering the major ion abundance (Table 1). Nitrate (NO_3^{-}) concentrations are generally within the WHO guideline value of 50 mg/L for all the samples except one sample from a hand-dug well in Yeji Township, which has concentration up to 70.6 mg/L. The high NO_3^{-} concentration in this hand-dug well is due to anthropogenic activities like agrochemical applications on farms around the Yeji Township. Boron (B) concentrations varied from 0.05 to 3.37 mg/L with an average concentration of 0.50 mg/L. This implies that groundwater in the semi-arid Pru Basin exceeds the maximum permissible limit (0.5 mg/L) of B in drinking water provided by the World Health Organization, W.H.O (2017). Twenty-two samples comprising of 4 boreholes and 18 hand-dug wells have high B concentrations when compared with the threshold value of 0.5 mg/L. The B enrichment may be due to the dominance of ion exchange reactions in the aquifer. The remaining anions such as CO_3^{2-} and SO_4^{2-} are within the permissible limits. The orders of concentration of the major cations and anions are $Na^{+} > Ca^{2+} > Mg^{2+} > K^{+}$ and $Cl^{-} > HCO_3^{-} > SO_4^{2-}$, respectively (Fig. 2).

4.2. Hydrochemical facies

Identifying the hydrochemical facies in an aquifer can help reveal mechanisms of both occurrence and salinization and possibly unravel the paleoenvironmental history of the groundwater system. Piper

Table 1
Concentrations of hydrochemical parameters in groundwater of the semi-arid Pru Basin and Revelle Index for groundwater salinization (all parameters are measured in mg/L except pH, temperature: ºC, EC: μS/cm, bdl: below detection limit, RI = Revelle index).

Sample ID	Location	pH	Temp.	EC	TDS	Na^+	K^+	Mg^{2+}	Ca^{2+}	Cl^-	SO_4^{2-}	HCO_3^-	CO_3^{2-}	NO_3^-	F^-	B	RI
PJ001	Perimukyeae 1	8.34	28.4	942	848	262	3.00	36.7	44.3	476	5.03	395	2.10	bdl	0.91	0.74	2.05
PJ002	Perimukyeae 2	8.34	27.5	852	767	297	2.72	14.9	24.1	306	6.65	382	2.10	bdl	0.85	1.32	1.36
PJ003	Peprabon	8.63	28.1	636	572	220	2.55	26.5	14.5	81.4	2.43	523	13.5	bdl	0.72	0.43	0.25
PJ004	Nyansebu No. 2	8.09	28.3	762	686	199	2.88	30.1	61.5	168	0.01	512	bdl	bdl	0.52	0.43	0.56
PJ005	Beposo 1	8.27	28.1	582	524	106	2.63	38.8	43.9	96.4	17.8	414	bdl	0.81	0.35	0.16	0.40
PJ006	Beposo 2	8.2	28.3	546	491	118	2.36	24.1	58.5	23.2	2.77	534	bdl	bdl	0.41	0.24	0.07
PJ007	Nyomoase	8.19	27.7	630	567	144	2.40	21.1	55.3	104	17.1	403	bdl	33.7	0.40	0.24	0.44
PJ008	Baakya	8.13	28.3	1908	1717	446	4.50	51.2	183	1131	1.93	361	bdl	bdl	bdl	0.63	5.39
PJ009	Adeemra	7.77	27.8	7914	7123	2115	9.27	27.2	505	4671	50.2	121	bdl	43.8	bdl	2.72	66.2
PJ010	Bolga Nkwanta	8.01	28.5	636	572	179	2.54	20.5	44.5	115	4.57	440	bdl	bdl	0.65	0.35	0.45
PJ011	Prang	8.17	29.9	612	551	206	2.73	16.3	33.8	26.2	15.9	578	bdl	2.99	0.88	0.59	0.08
PJ012	Prang	8.50	29.2	516	464	196	2.10	9.82	13.2	22.2	7.90	478	8.40	bdl	0.48	0.38	0.08
PJ013	Labun Quarters	8.51	28.9	948	853	295	2.79	50.3	27.2	252	1.39	612	10.5	bdl	0.91	0.98	0.68
PJ014	Labun Kofi Baasari	8.05	29.9	2190	1971	675	2.22	11.7	94.5	1417	5.07	243	bdl	2.81	1.21	1.40	10.0
PJ015	Parambo No. 1	8.5	31.5	576	518	240	1.49	0.24	8.16	20.5	61.4	461	7.20	bdl	2.70	1.46	0.07
PJ016	Parambo Sawaba	8.35	30.5	576	518	187	2.28	30.1	18.0	5.57	7.34	602	4.20	2.13	0.55	0.23	0.02
PJ017	Bomoden	8.53	27.6	492	443	132	1.96	15.3	23.9	58.2	3.97	389	7.20	bdl	0.50	0.20	0.25
PJ018	Echamba	8.27	27.7	510	459	142	1.98	9.94	24.6	54.5	14.8	395	bdl	bdl	0.98	0.30	0.24
PJ019	Sabaalo	8.23	30.1	642	578	225	2.23	17.5	28.8	25.7	23	604	bdl	bdl	0.50	0.52	0.07
PJ020	Burkina Bumbo	7.97	28.4	2604	2344	601	2.64	84.8	198	1787	50.6	214	bdl	4.53	2.23	1.80	14.4
PJ021	Bankama	8.06	29.5	2076	1868	609	1.78	28.2	101	1341	13.8	224	bdl	4.44	1.45	3.26	10.3
PJ022	Kranya Kuraa 1	8.14	29.3	588	529	198	1.89	8.67	29.3	74.6	7.41	465	bdl	bdl	0.51	0.41	0.28
PJ023	Kranya Kuraa 2	8.29	28.8	522	470	172	1.76	11.0	30.4	26.4	5.31	489	bdl	1.01	0.53	0.29	0.09
PJ024	Kajamansuo	8.03	29.4	570	513	134	1.91	17.7	46.0	75.7	19.3	427	bdl	0.65	0.88	0.53	0.30
PJ025	Kobiase	7.92	29.2	312	281	74.0	1.46	6.96	13.1	6.55	1.22	265	bdl	0.86	1.23	0.09	0.04
PJ026	Kakrunji	8.49	28.4	348	313	83.0	1.50	6.30	22.1	13.5	1.74	301	5.10	bdl	0.72	0.11	0.07
PJ027	Kapua	8.29	29.6	660	594	193	2.19	20.5	41.0	103	7.83	506	bdl	bdl	0.70	0.27	0.35
PJ028	Chekronmo Nkwanta	8.04	30.4	2418	2176	683	1.99	26.1	130	1652	19.5	179	bdl	3.16	1.20	3.37	15.8
PJ029	Kapua	8.07	30.5	378	340	58.0	10.8	13.4	33.2	30.4	5.38	282	bdl	0.78	0.25	0.11	0.19
PJ030	Yeji (Catholic Hospital) 1	8.23	29.6	528	475	125	2.27	14.5	40.8	78.4	4.84	354	bdl	33.8	0.27	0.10	0.38
PJ031	Yeji (Catholic Hospital) 2	8.36	29.8	540	486	174	2.23	10.8	35.8	26.7	5.30	465	3.00	33.2	0.41	0.13	0.10
PJ032	Yeji (Township) 1	8.27	29.8	588	529	171	2.28	15.0	47.1	26.4	5.25	514	bdl	32.6	0.37	0.10	0.09
PJ033	Yeji (Township) 2	8.17	30.2	744	670	230	2.14	12.8	49.9	84.4	11.9	529	bdl	70.3	0.40	0.23	0.27
PJ034	Kobre	8.36	29.6	1314	1183	466	1.91	13.1	25.2	552	48.2	429	3.00	3.80	1.46	1.59	2.18
PJ035	Kojo Boffour	8.35	30.0	366	329	94.0	1.83	8.90	20.3	34.5	3.48	333	2.10	bdl	bdl	0.14	0.18
PJ036	Yeji (Township) 3	8.36	29.9	324	292	70.0	1.69	11.1	19.4	4.93	2.19	286	bdl	bdl	0.29	0.09	0.03
PJ037	Yeji (Township) 4	8.25	29.9	396	356	97.0	1.80	13.2	25.5	12.6	4.04	361	bdl	2.22	0.27	0.12	0.06
PJ038	Yeji (Township) 5	8.11	29.5	372	335	86.0	1.61	10.4	26.1	5.92	5.24	331	bdl	bdl	0.31	0.11	0.03
PJ039	Nakpei	8.41	29.6	624	562	172	2.03	29.1	33.5	103	9.33	457	5.10	1.06	0.79	0.16	0.38
PJ040	Kudjokrom	8.40	29.0	570	513	186	1.59	18.1	27.3	40.1	9.46	512	6.30	0.62	0.68	0.16	0.13
PJ041	Kadue	8.37	29.6	528	475	141	2.12	24.2	35.9	20.9	2.81	514	4.20	3.05	0.36	0.09	0.07
PJ042	Agyentruwa	8.35	28.4	726	653	240	1.39	14.7	29.3	162	10.5	470	3.00	1.40	1.11	0.25	0.58
PJ043	Tsrikrono/Paye Kuraa	8.15	29.1	456	410	124	1.41	14.0	39.3	2.51	3.55	465	bdl	0.76	0.59	0.1	0.01
PJ044	Kabende	8.21	28.5	492	443	118	1.40	17.7	50.0	9.90	2.18	487	bdl	bdl	0.52	0.09	0.03
PJ045	Hiampe	8.28	28.3	768	691	252	1.53	16.4	39.4	125	26.4	561	bdl	bdl	0.68	0.56	0.38
PJ046	Tarakpa	8.40	28.4	780	702	279	1.30	4.49	20.5	213	21.4	416	4.20	1.64	1.18	0.98	0.86

Sample ID	Location	pH	Temp.	EC	TDS	Na^+	K^+	Mg^{2+}	Ca^{2+}	Cl^-	SO_4^{2-}	HCO_3^-	CO_3^{2-}	NO_3^-	F^-	B	RI
PJ047	Wokwansua	8.34	29.1	468	421	135	1.37	12.9	31.8	5.99	18.8	444	3.00	bdl	0.63	0.26	0.02
PJ048	Kwadjoabe 1	8.6	28.4	792	713	285	1.36	11.3	21.0	149	53.9	517	11.4	1.93	1.01	0.91	0.48
PJ049	Kwadjoabe 2	8.35	28.2	768	691	280	1.32	8.16	17.5	133	49.4	497	3.00	bdl	1.35	0.85	0.46
PJ050	Beposo No. 3	8.19	29.7	540	486	170	1.25	10.7	35.3	21.2	6.02	517	bdl	bdl	0.52	0.25	0.07
PJ051	Adjalaja Beposo 1	8.28	29.6	522	470	187	1.27	7.42	18.8	16.2	3.61	510	bdl	0.78	0.64	0.26	0.05
PJ052	Adjalaja Beposo 2	8.14	29.0	534	481	164	1.21	13.8	38.5	8.93	3.64	544	bdl	bdl	0.48	0.12	0.03
PJ053	Adjalaja Beposo 3	8.32	29.1	480	432	154	1.20	14.8	20.9	7.79	4.42	478	2.10	bdl	0.39	0.11	0.03
PJ054	Adjalaja	8.53	28.0	558	502	165	1.21	22.7	29.2	63.2	5.25	461	8.40	0.83	0.48	0.14	0.23
PJ055	Bawa Kuraa	8.39	28.2	552	497	167	1.18	7.92	34.0	93.5	9.66	378	3.00	bdl	1.46	0.34	0.42
PJ056	Ankerekuka	8.27	28.1	684	616	195	1.30	21.1	42.0	125	5.25	493	bdl	2.20	0.82	0.22	0.44
PJ057	Sele	8.61	29.2	744	670	255	1.18	18.1	33.8	75.8	24.5	641	14.7	bdl	1.18	0.69	0.19
PJ058	Dogo Dakyi	8.12	28.0	306	275	34.0	1.19	10.8	59.8	1.63	2.02	271	bdl	bdl	0.38	0.06	0.01
PJ059	Dogodaji	8.11	12.0	324	292	25.0	1.19	11.4	78.3	1.36	2.53	292	bdl	bdl	0.35	0.05	0.01
PJ060	Abaase Dadamu	8.37	32.1	984	886	258	1.36	50.5	45.8	345	51.8	442	4.20	4.60	bdl	0.12	1.32
PJ061	Abaase Newtown 1	8.36	33.6	438	394	75.0	1.23	23.8	62.0	14.55	15.6	389	3.00	8.45	0.37	0.12	0.06
PJ062	Abaase Newtown 2	8.30	33.2	390	351	68.0	1.18	18.7	56.0	5.64	5.06	369	0.90	4.80	0.31	0.06	0.03
PJ063	Hiampe	8.33	29.0	654	589	216	1.21	16.4	28.2	67.0	23.7	548	3.00	1.13	0.77	0.33	0.21
PJ064	Fawoman 1	8.60	32.0	486	437	137	1.16	14.0	28.6	61.0	1.80	378	9.30	bdl	1.29	0.17	0.26
PJ065	Fawoman 2	8.30	20.0	384	346	123	1.14	5.54	18.4	29.8	0.02	307	0.90	bdl	0.80	0.15	0.17
PJ066	Dumase Kora	8.40	18.4	462	416	138	1.18	16.8	27.3	54.5	6.81	359	4.20	0.65	0.60	0.07	0.26
PJ067	Wurukasa	8.54	13.0	798	718	320	0.98	2.44	10.0	220	72.6	348	7.20	bdl	3.40	1.80	1.05
PJ068	Asibene	8.08	12.6	2406	2165	664	2.75	29.0	162	1667	5.29	167	bdl	bdl	0.76	1.62	17.2
PJ069	Beposo No. 1	8.34	11.8	504	454	108	1.49	21.1	45.3	18.0	4.52	495	3.00	0.84	0.51	0.13	0.06
PJ070	Beposo No. 2A	8.46	13.0	450	405	110	1.38	18.4	23.1	11.6	4.95	427	6.30	3.20	0.43	0.13	0.05
PJ071	Beposo No. 2B	8.50	13.1	468	421	114	1.62	23.0	20.0	13.0	3.49	453	7.20	bdl	0.38	0.09	0.05
PJ072	Beposo No. 2C	8.50	13.6	546	491	147	1.41	14.0	36.4	17.1	4.24	544	9.30	0.63	0.48	0.18	0.05
PJ073	Beposo No. 2D	8.42	13.0	432	389	95.0	1.38	20.7	23.9	32.0	3.87	373	4.20	bdl	0.39	0.11	0.14
PJ074	Beposo No. 2E	8.46	13.0	486	437	121	1.63	21.9	27.5	14.2	4.37	480	7.20	bdl	0.47	0.09	0.05
PJ075	Beposo No. 2F	8.29	13.3	570	513	147	1.53	16.8	42.1	22.0	4.12	555	bdl	bdl	0.53	0.23	0.07
PJ076	Beposo No. 2G	8.37	12.7	588	529	191	1.61	15.0	38.5	30.2	2.45	565	4.20	bdl	0.48	0.18	0.09
PJ077	Ajalaja 1	8.27	11.2	690	621	199	1.75	21.4	56.3	89.5	3.70	564	bdl	1.89	0.56	0.34	0.27
PJ078	Ajalaja 2	8.15	12.2	852	767	249	1.61	16.2	61.7	241	3.25	470	bdl	bdl	0.46	0.61	0.88
PJ079	Kumfia 1	8.24	13.1	492	443	77.0	2.55	23.5	53.3	37.8	53.3	320	bdl	33.1	bdl	0.15	0.20
PJ080	Kumfia 2	8.02	13.6	372	335	78.0	1.52	11.3	26.5	6.29	35.5	296	bdl	bdl	0.23	0.11	0.04
PJ081	Sella No 1	8.49	13.0	756	680	260	1.85	25.8	36.7	92.6	15.7	630	10.5	bdl	0.61	1.25	0.24

Table 2
Statistical summary of hydrochemical parameters in groundwater of the semi-arid Pru Basin (STD = Standard Deviation; SABSL = Samples Above Standard Limit).

Parameter	Sample No.	Minimum	Maximum	Average	STD	WHO (2017)	SASL
pH	81	7.77	8.63	8.29	0.17	6.5–8.5	8
Temp.	81	11.2	33.6	25.8	6.77	NA	
EC	81	306	7914	797	933	2500	2
TDS	81	275	7123	717	840	500	41
Na^+	81	25.2	2115	226	254	200	26
K^+	81	0.98	10.8	2.00	1.42	200	None
Ca^{2+}	81	8.16	505	48.2	61.6	200	1
Mg^{2+}	81	0.24	84.8	18.8	12.3	NA	
Cl^-	81	1.36	4671	240	634	250	11
SO_4^{2-}	81	0.01	72.6	13.2	16.4	200	None
HCO_3^-	81	121	641	430	113	NA	
CO_3^{2-}	81	0.00	14.7	2.76	3.64	NA	
NO_3^-	81	0.00	70.3	4.34	11.8	50	1
F^-	81	0.00	3.40	0.70	0.55	1.5	3
B	81	0.05	3.37	0.50	0.68	0.5	22

Table 3
Pearson's correlation analysis of the hydrochemical parameters in groundwater of the semi-arid Pru Basin (values in bold indicate correlation coefficients ≥0.70).

	pH	Temp.	EC	TDS	Na^+	K^+	Mg^{2+}	Ca^{2+}	Cl^-	SO_4^{2-}	HCO_3^-	CO_3^{2-}	NO_3^-	F^-	B
pH	1.00														
Temp.	−0.10	1.00													
EC	−0.45	0.05	1.00												
TDS	−0.45	0.05	1.00	1.00											
Na^+	−0.39	0.07	**0.99**	**0.99**	1.00										
K^+	−0.40	0.13	0.56	0.56	0.52	1.00									
Mg^{2+}	−0.16	0.03	0.34	0.34	0.27	0.24	1.00								
Ca^{2+}	−0.55	0.01	**0.95**	**0.95**	**0.89**	0.58	0.41	1.00							
Cl^-	−0.49	0.05	**0.99**	**0.99**	**0.97**	0.54	0.38	**0.94**	1.00						
SO_4^{2-}	0.02	0.02	0.33	0.33	0.37	0.07	0.09	0.22	0.30	1.00					
HCO_3^-	0.48	0.00	−0.44	−0.44	−0.38	−0.30	−0.06	−0.48	−0.55	−0.12	1.00				
CO_3^{2-}	0.83	−0.11	−0.14	−0.14	−0.08	−0.19	0.01	−0.27	−0.18	0.13	0.35	1.00			
NO_3^-	−0.23	0.10	0.32	0.32	0.30	0.28	0.01	0.35	0.27	0.16	−0.11	−0.20	1.00		
F^-	0.17	0.06	0.06	0.06	0.14	−0.21	−0.06	−0.10	0.09	0.51	−0.08	0.23	−0.22	1.00	
B	−0.26	0.06	**0.70**	**0.70**	**0.75**	0.25	0.23	0.54	**0.73**	0.46	−0.39	−0.01	0.06	0.52	1.00

(1953) diagram indicates that the groundwater types in the semi-arid Pru Basin spread within Na-HCO3, Na-HCO3-Cl, Na-Ca-HCO3, and Na-Mg-HCO3 types in a decreasing order of abundance (Fig. 3). The Na-HCO3 type reflects input from ion exchange reactions in the aquifer (Song et al., 2007) and chemical weathering of silicate minerals. The Na-HCO3-Cl groundwater type is dominant in areas towards the Volta Lake, which are under threat of anthropogenic activities such as farming involving the use of agrochemicals. The Na-Ca-HCO3 and Na-Mg-HCO3 water types indicate aquifer recharge water (Gopinath et al., 2014). Since groundwater from recharge areas experiences lower rates of water-sediment interaction (Stuyfzand, 1999), this accounted for the paucity of the Na-Ca-HCO3 and Na-Mg-HCO3 water types as compared to the other water types, which are mainly related to discharge areas.

Matthes (1982) characterized the hydrochemical facies of groundwater using indices rather than the usual Piper ternary diagram. He proposed the base-exchange index (r1) using Na^+, Cl^- and SO_4^{2-} parameters (eq. 3) with their concentrations in meq/L and the meteoric genesis index (r2) using K^+, Na^+, Cl^- and SO_4^{2-} parameters (eq. 4) with concentrations in meq/L. With r1 < 1, the water facies is said to be that of $Na^+ - SO_4^{2-}$, whiles r1 > 1 implies that the water is of $Na^+ - HCO_3^-$ type. Also, r2 < 1 means that there was a deeper percolation of meteoric water and hence longer residence time and r2 > 1 indicates that meteoric water percolation was up to shallow levels (Matthes, 1982).

$$\text{Base} - \text{exchange index (r1)} = \left(Na^+ - Cl^-\right)/SO_4^{2-} \quad (3)$$

$$\text{Meteoric genesis index (r2)} = \left(K^+ + Na^+\right) - Cl^-/SO_4^{2-} \quad (4)$$

The calculated r1 indices for the studied samples show that 8 samples representing approximately 10% of the collected samples fall in the $Na^+ - SO_4^{2-}$ type field and the remaining 73 samples representing approximately 90% of the collected samples are $Na^+ - HCO_3^-$ water types (Fig. 4a). By the indices calculated (Table 4), the water facies in the area show a dominant $Na^+ - HCO_3^-$ water type and minor amount of $Na^+ - SO_4^{2-}$ water type (Fig. 4a). The r2 calculations on the other hand show that majority of the samples have r2 values <1 implying that they had longer residence time via deeper percolation (Fig. 4b). The higher percentage of the samples with r2 < 1 accounts for the high TDS, Na^+, Cl^-, and HCO_3^- concentrations observed in the samples since there will be enough time for ion exchange reactions in the aquifer for the ion enrichment.

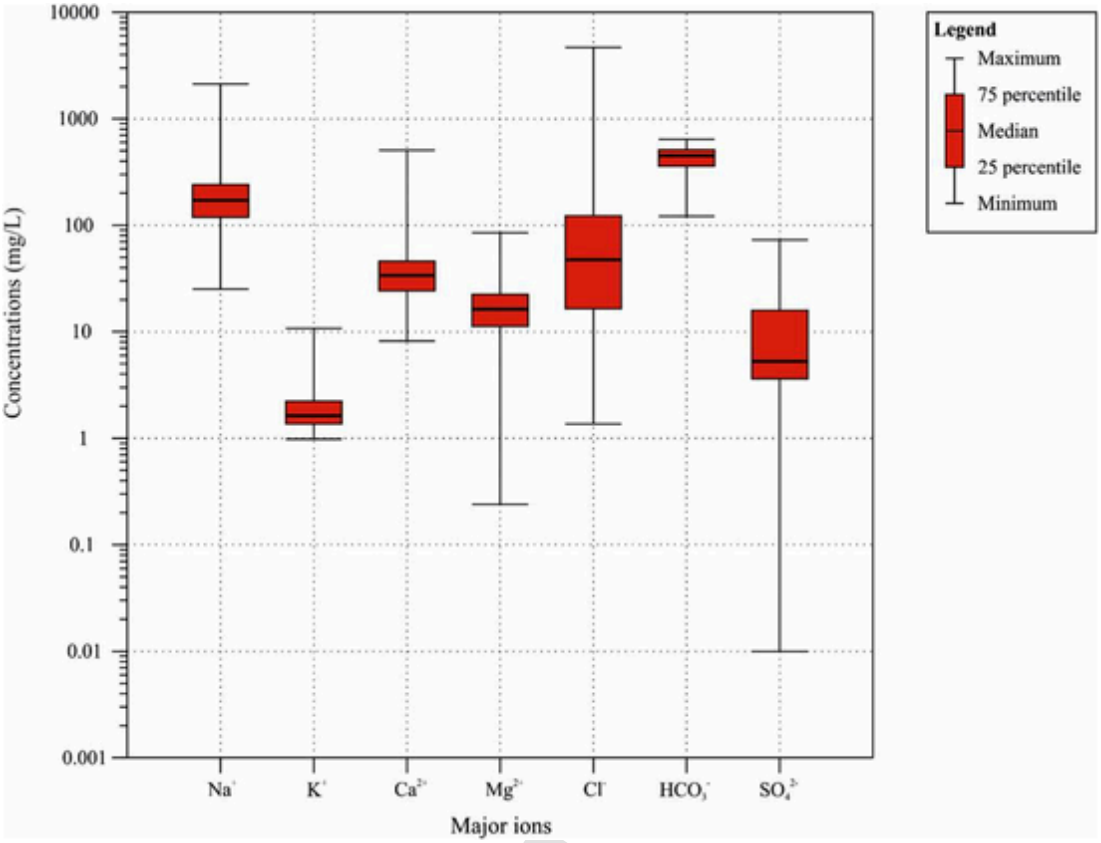

Fig. 2. Box and whisker plot of the major ion concentrations in groundwater of the semi-arid Pru Basin.

4.3. Spatial distribution of hydrochemical parameters

Spatial distribution maps of the various hydrochemical parameters are presented in Fig. 5. From the maps, it is observed that higher pH values are found in samples collected from the northwestern and central parts of the study area (Fig. 5a). The high TDS and Na^+ concentrations given in Table 1 are mainly around the southwestern fringe of the study area in Peprabon community and its surroundings (Fig. 5b and c). The K^+ distribution map also shows high values in the northern and southern parts of the semi-arid Pru Basin (Fig. 5d). High Ca^{2+} content is only observed in the southwestern peripheral (Fig. 5e) just like the TDS and Na^+ concentrations. The Mg^{2+} distribution map indicates that high concentrations are only restricted to the northwestern domain of the semi-arid Pru Basin (Fig. 5f), which is dominated by limestones and dolomites of the Oti/Pendjari Group of the Voltaian Supergroup. The Cl^- distribution map shows high Cl^- content mainly in the southwestern part of the semi-arid Pru Basin consistent with the high TDS content observed in the same area (Fig. 5g). This may suggest that there is interplay of processes like salinization and anthropogenic activities in the southwestern part of the basin. The northwestern part of the basin also shows high SO_4^{2-} content (Fig. 5h) and could be interpreted as a result of weathering of gypsum from the carbonate lithologies of the Oti/Pendjari Group. Among all the hydrochemical parameters, only HCO_3^- shows high content in almost all the parts of the semi-arid Pru Basin (Fig. 5i). This might be as result of the homogeneous dominance of carbonate rocks in the basin. The NO_3^- distribution map reveals that high NO_3^- in the semi-arid Pru Basin is only common in the northeastern part of the basin towards Yeji community, where farming activities are dominant (Fig. 5j). Nevertheless, slightly high NO_3^- content is observed in the southwestern part, especially towards Peprabon community (Fig. 5j). F^- concentrations appear to be high in the northwestern and eastern fringes of the study area, particularly in Parambo No. 1, Burkina Bumbo and Wurukasa (Fig. 5k). This suggests that the inhabitants in these communities are prone to the threat of dental fluorosis should they keep drinking water from those hand-dug wells. The high B content of groundwater in the semi-arid Pru Basin is mainly in the northern, eastern, southern and northwestern parts (Fig. 5l).

4.4. Multivariate statistics and geochemical modeling

The R-mode FA resulted in four factors with eigenvalues >1 (Table 4). These factors explained 76.0% of the total variance of all the hydrochemical parameters analyzed in this study. Factor 1, which explains about 37.6% of the total variance (Table 4) is contributed by EC, TDS, Na^+, K^+, Ca^{2+}, Mg^{2+}, and Cl^- (Fig. 6). Factor 2 explains 15.5% of the sample variance (Table 4) and loads positively on pH, HCO_3^- and CO_3^- (Fig. 6). Factor 3 accounts for 14.6% of the variance (Table 5) and mainly associated with SO_4^{2-}, F^- and B (Fig. 6). Factor 4 explains about 8.32% of the total variance of the dataset (Table 4) and is strongly associated with temperature and NO_3^- (Fig. 6).

Statistical summary of the calculated saturation indices (SI) of the identified mineral phases in the groundwater are presented in Table 5. All the studied samples are saturated with respect to calcite (0.08–1.36, average of 0.90) and dolomite (0.07–2.97, average of 1.79). The samples are under-saturated with respect to gypsum (−5.79 to −1.71) and anhydrite (−6.03 to −1.92) (Table 5). Some of the studied samples also appear to be saturated with respect to aragonite (−0.06 to 1.22, average of 0.76) and talc (−4.54–5.54, average of 1.99) (Table 5). However, all the samples are under-saturated with respect to halite (−9.01 to −3.75) and fluorite (−2.68 to −0.27) (Table 5). The calculated SI values of minerals by PHREEQC also show that some samples

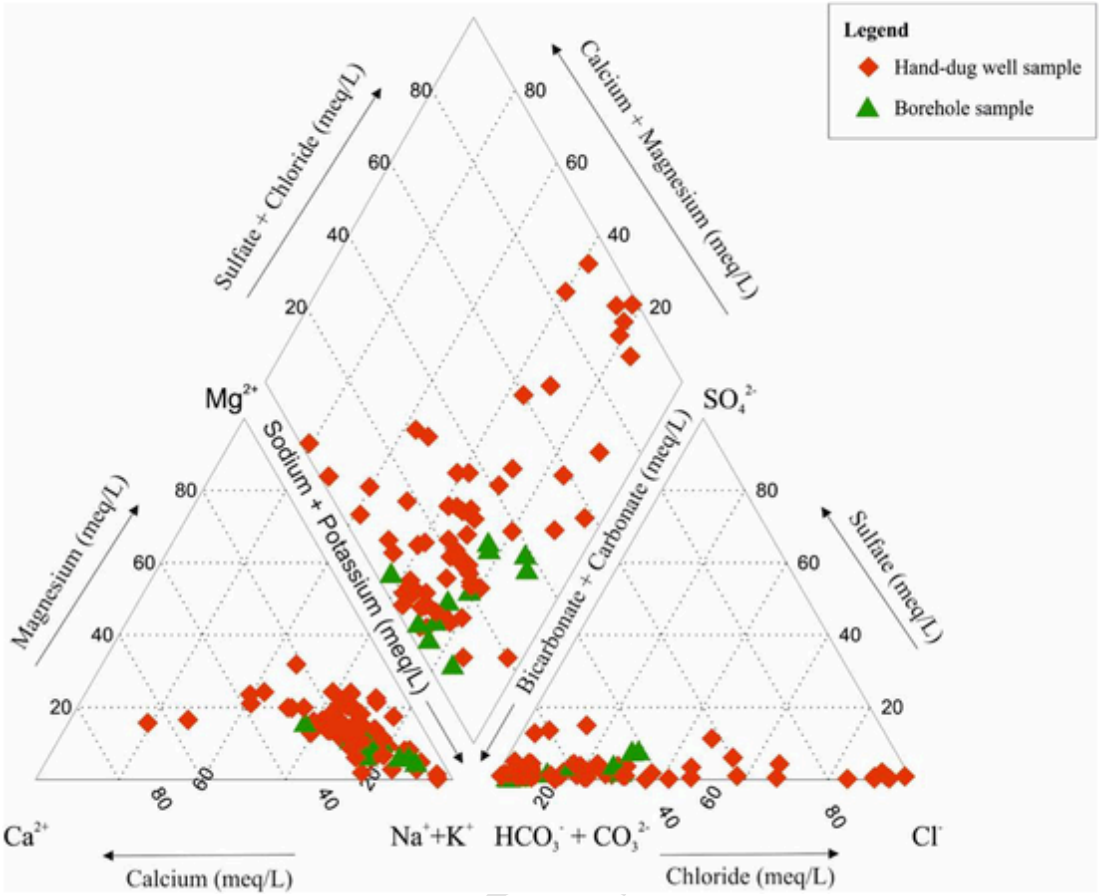

Fig. 3. Piper (1953) diagram showing the various hydrochemical facies in the groundwater.

are saturated with respect to silicate minerals such as albite (−5.60–0.27, average of −2.73), chalcedony (−1.24–0.28, average of −0.47), and quartz (−0.82–0.75, average of −0.04) (Table 5).

5. Discussion

5.1. Processes controlling groundwater chemistry

5.1.1. Ion exchange reactions

Schoeller (1965) used chloro-alkaline indices CAI – 1 and CAI – 2 to indicate forward ion exchange and reverse ion exchange reactions, and these indices have been extensively used in evaluating how ion exchange governs the occurrence of groundwater (Ako et al., 2012; Emenike et al., 2020). Positive CAI – 1 (eq. 5) and CAI – 2 (eq. 6) is indicative of reverse ion exchange reaction where Na^+ and K^+ replace Ca^{2+} and Mg^{2+} ions whereas it becomes forward ion exchange reaction when CAI – 1 and CAI – 2 values are negative with Ca^{2+} and Mg^{2+} replacing Na^+ and K^+ in the process. The 81 groundwater samples of the semi-arid Pru Basin show that about 68% of the samples are with negative CAI – 1 and CAI – 2 values indicating a dominant forward ion exchange reaction with Ca^{2+} and Mg^{2+} replacing Na^+ and K^+ in the process due to the presence of dolomitic rocks in the area. This process is further observed in Fig. 7a, which involves CAI – 1 values indicating both forward and reverse ion exchange processes with dominant forward ion exchange. However, reverse ion exchange reaction is observed as the dominant process in the CAI – 2 diagram (Fig. 7b). It can thus, be concluded that on a basin scale, both forward and reverse ion exchange reactions control groundwater chemistry in the semi-arid Pru Basin. This is supported by the average CAI – 1 and CAI – 2 values (Table 4).

$$\text{CAI 1} = \text{Cl} - \left(\text{Na}^+ + \text{K}^+\right)/\text{Cl} \quad (5)$$

$$\text{CAI 2} = \text{Cl} - \left[\left(\text{Na}^+ + \text{K}^+\right)/\text{SO}_4^{2-}\right] + \text{HCO}_3^- + \text{CO}_3^{2-} + \text{NO}_3^- \quad (6)$$

Moreover, a plot of $Ca^{2+} + Mg^{2+}$ versus $HCO_3^- + SO_4^{2-}$ reveals the dominance of ion exchange reactions, mainly forward ion exchange in the aquifer since most of the samples shift to the right due to an excess of $HCO_3^- + SO_4^{2-}$ (Fig. 8a). If reverse ion exchange was the dominant process, the samples would have shifted to the left due to an excess of $Ca^{2+} + Mg^{2+}$ over $HCO_3^- + SO_4^{2-}$ (McLean and Jankowski, 2000), via the reaction below (eq. 7). Nevertheless, three hand-dug well samples plot in the reverse ion exchange field (Fig. 7a).

$$2\text{Na}^+ + \text{Ca(Mg) clay} \leftrightarrow \text{Na–clay} + \text{Ca}^{2+}\left(\text{Mg}^{2+}\right) \quad (7)$$

Fig. 8b confirms that reverse ion exchange is also a common process in the aquifer system of the semi-arid Pru Basin. This plot involves Mg^{2+} versus $Ca^{2+} + Mg^{2+}$, where all the samples shift to the left except two that shifted to the right, indicating that reverse ion exchange predominates the system than forward ion exchange. Further confirmation of this is observed in the plot of Ca^{2+} versus $Ca^{2+} + SO_4^{2-}$, where all the samples plot in the reverse ion exchange field save for two samples that plot in the forward ion exchange field (Fig. 8c). But the plot of Na^+ versus Cl^- equilibrates the two processes in the aquifer system (Fig. 8d), implying that both forward ion exchange and reverse ion exchange reactions are the dominant processes influencing groundwater chemistry in the semi-arid Pru Basin.

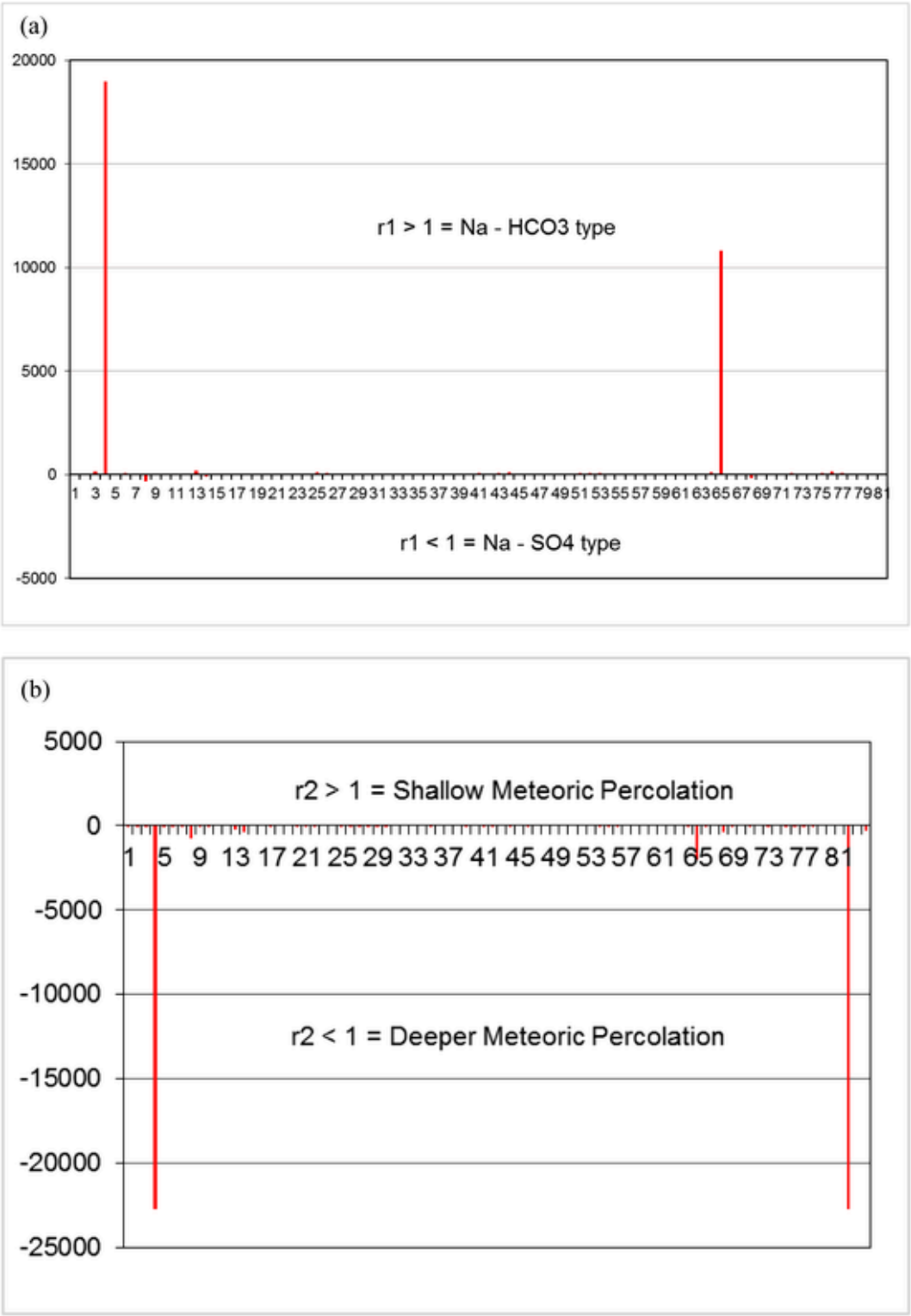

Fig. 4. Base-exchange indices (r1) and (b) meteoric genesis indices (r2) showing the various water types and percolation depth.

5.1.2. Water – rock interaction

The samples in this study were plotted on the Gibbs (1970) diagrams to identify the principal geochemical controls of the groundwater chemistry. On the cationic diagram, which involves.

TDS versus Na/(Na + Ca), majority of the samples plot in the rock weathering dominance field whereas a few samples plot in the evaporation-crystallization dominance field (Fig. 9a). This suggests that chemical weathering of rocks and dissolution of minerals as well as evaporation are the principal controls of the groundwater chemistry. Similar trend is observed in the anionic diagram (Fig. 9b) that involves TDS versus Cl/(Cl + HCO3). Nevertheless, the increase in TDS against Na/(Na + Ca) and Cl/(Cl + HCO3) in both diagrams implies that other processes such as ion exchange reactions are also controls of the

Table 4
Rotation plot from R-mode factor analysis using principal component analysis as initial extraction technique (bold values indicate good positive loadings for each factor).

Parameter	Factor 1	Factor 2	Factor 3	Factor 4
pH	−0.31	**0.87**	0.10	−0.13
Temp.	−0.08	−0.07	0.15	**0.74**
EC	**0.94**	−0.19	0.22	0.11
TDS	**0.94**	−0.19	0.22	0.11
Na^+	**0.90**	−0.14	0.30	0.13
K^+	**0.62**	−0.18	−0.20	0.28
Mg^{2+}	**0.53**	0.12	−0.13	−0.14
Ca^{2+}	**0.92**	−0.30	0.02	0.08
Cl^-	**0.92**	−0.27	0.24	0.05
SO_4^{2-}	0.22	0.11	**0.70**	0.19
HCO_3^-	−0.34	**0.64**	−0.22	0.12
CO_3^{2-}	0.01	**0.90**	0.19	−0.17
NO_3^-	0.30	−0.07	−0.15	**0.67**
F^-	−0.10	0.07	**0.90**	−0.11
B	0.58	−0.16	**0.67**	−0.06
Total Initial Eigenvalue	6.69	2.27	1.36	1.08
Percentage of variance	37.6	15.5	14.6	8.32
Cumulative % of variance	37.7	53.1	67.7	76.0

groundwater chemistry (Li et al., 2016). Aside using the traditional bivariate plot of Gibbs to infer the relation between the host rock and the groundwater, a number of ratios have been used to elucidate the effect of water – rock interaction as a mineralization process of groundwater. Cl/Σ anions, Na^+/Cl^-, $Na^+/(Na^+ + Ca^{2+})$ and $Mg^{2+}/(Ca^{2+} + Mg^{2+})$ have been used to deduce the effect of silicate weathering (Naseem et al., 2010; Kumar et al., 2018). The <1 value of Cl/Σ anions is indicative of silicate mineral weathering (Kumar et al., 2018) in the basin (Table 6). This is supported by the <1 values of $Na^+/(Na^+ + Ca^{2+})$ and $Mg^{2+}/(Ca^{2+} + Mg^{2+})$ (Table 6). In addition, Moghaddam and Fijani (2008) indicated that the $Mg^{2+}/(Ca^{2+} + Mg^{2+})$ also differentiates between the contribution of the different rock types in area. Hence, the average value of $Mg^{2+}/(Ca^{2+} + Mg^{2+})$ (Table 6) is <1 supporting the input of ferromagnesian minerals from the adjacent mafic rocks of the Paleoproterozoic Birimian Supergroup in the area. The effect of silicate mineral weathering and for that matter water – rock interaction, is again emphasized by the high average Na^+/Cl^- value (> 1) in the area (Table 6). The positive correlation between Ca^{2+} and Na^+ and K^+ (Table 3) suggests that cation exchange reaction within crystalline aquifers is a dominant process, where water – rocks reaction played a significant role in the chemistry of the groundwater within the semi-arid Pru Basin. The semi-arid Pru Basin, which is largely within the Oti/Pendjari Group of the Voltaian Supergroup (Fig. 1b), overlies feldspathic and quartzitic sandstones, which also unconformably overly the basement Birimian rocks. These feldspathic sandstones as well as the Birimian rocks contain silicate minerals as their constituent minerals and thus, one cannot preclude possible water – rock interaction as a contributory factor to groundwater chemistry in the area. This proposition is supported by the high EC level, which indicates high water residence time in the aquifer that possibly allowed enough time for the rock minerals to react with the groundwater.

The fact that silicate weathering plays a critical role in the groundwater chemistry is supported by the bivariate plot involving $Ca^{2+} + Mg^{2+}$ versus $HCO_3^- + SO_4^{2-}$ (Fig. 8a). In this plot, samples below the 1:1 equiline are attributed to silicate weathering whilst those above the 1:1 equiline might have resulted from carbonate mineral weathering of calcite, gypsum, or dolomite (Chegbeleh et al., 2020). Such process involves reaction of atmospheric carbonic acid with the water to dissolve the carbonate minerals, which preferentially releases Ca^{2+} and Mg^{2+} in the water. This chemical process is further highlighted in Fig. 8b for the weathering of dolomite and Fig. 8c for the weathering of gypsum. The samples that plot near or along the 1:2 line may be as a result of dolomite and gypsum weathering. On the plot of Na^+ versus Cl^- (Fig. 8d), three processes can be observed; the first two are reverse and forward ion exchange reactions for the samples with higher Na^+ as explained earlier, whereas the third is saline water intrusion for the samples with higher Cl^-. Majority of the samples plot close to the 2:1 line, which may indicate the effect of halite dissolution on groundwater chemistry. However, halite is less common in the study area and thus, anthropogenic activities might be enriching Cl^- in the groundwater. Using the Na-normalized Ca versus HCO3 plot (Fig. 8e) of Gaillardet et al. (1999), all the samples range from being influenced by silicate weathering, evaporate dissolution and carbonate dissolution in a decreasing order of magnitude. Also, on a Na-normalized Ca versus Mg plot (Fig. 8f), it is observed that although majority of the Mg content of the groundwater may have been derived from carbonate (dolomite) dissolution, a significant fraction may have come from silicate and evaporate dissolution.

5.1.3. Salinization

The computed Revelle index (RI) values ranged from 0.01 to 66.2 (Table 1). The RI assessment of the level of groundwater salinization in the semi-arid Pru Basin indicates that about 19.8% of the groundwater samples with RI values >0.5 is influenced by salinization. Therefore, in order to identify the potential sources of groundwater salinization in the semi-arid Pru Basin, ionic plots were produced. Ions such as Na^+, K^+, Ca^{2+}, Mg^{2+}, Cl^-, SO_4^{2-} and B have proven to be conservative tracers of groundwater salinization in any hydrogeological system (Gopinath et al., 2014). The effect of saline water intrusion and anthropogenic activities on groundwater chemistry is demonstrated in Fig. 10a. On this plot, the samples showing Na/Cl ratios ≤0.86 suggest that the groundwater is intruded by saline water whereas the samples with Na/Cl ratios ≥1 are likely to have been contaminated by anthropogenic sources (Naily, 2018; Sunkari et al., 2019). About 12.4% of the groundwater resources, mainly hand-dug wells in the semi-arid Pru Basin are affected by saline water intrusion when compared with saline water from the Volta River (Egbi et al., 2019), which serves as the major reservoir for the semi-arid Pru Basin, implying that saline water from adjacent aquifers may be contributing to groundwater salinization. Moreover, majority of the samples (87.7%) plot in the zone of anthropogenic pollution (Fig. 10a), implying that the groundwater salinization is largely influenced by anthropogenic sources like run-offs and infiltration from irrigable farm lands comparable to the study of Karunanidhi et al. (2020). From the spatial maps, the high Cl^- and TDS contents are restricted to the southwestern part of the basin (Fig. 5b and g), where there is no paucity of anthropogenic activities. Most of the rivers making up the Volta River drainage system are found in the southwestern part of the basin and the rural dwellers depend on them for irrigation farming as well as small-scale fishing. It is possible that leaching from the chemicals the farmers use in these activities may be the culprit for the groundwater salinization in the southwestern part of the basin. Abdalla (2016) proposed the use of Ca/(HCO3 + SO4) versus Na/Cl diagram to demarcate water that is influenced by saline water and base ion exchange as drivers of groundwater salinization. Therefore, on the Ca/(HCO3 + SO4) versus Na/Cl diagram, 10 samples representing 12.4% of the studied samples plot in the Cl-excess zone, which is the region of higher salinity, 70 samples representing 86.4% of the total samples plot in the Base Ion Exchange zone, whereas only 1 sample representing 1.23% of the total samples plot in the Ca-Excess zone (Fig. 10b). Certainly, this trend suggests that in addition to anthropogenic activities as discussed earlier, ion exchange reactions and saline water intrusion from adjacent aquifers are the principal controls of groundwater salinization in the semi-arid Pru Basin.

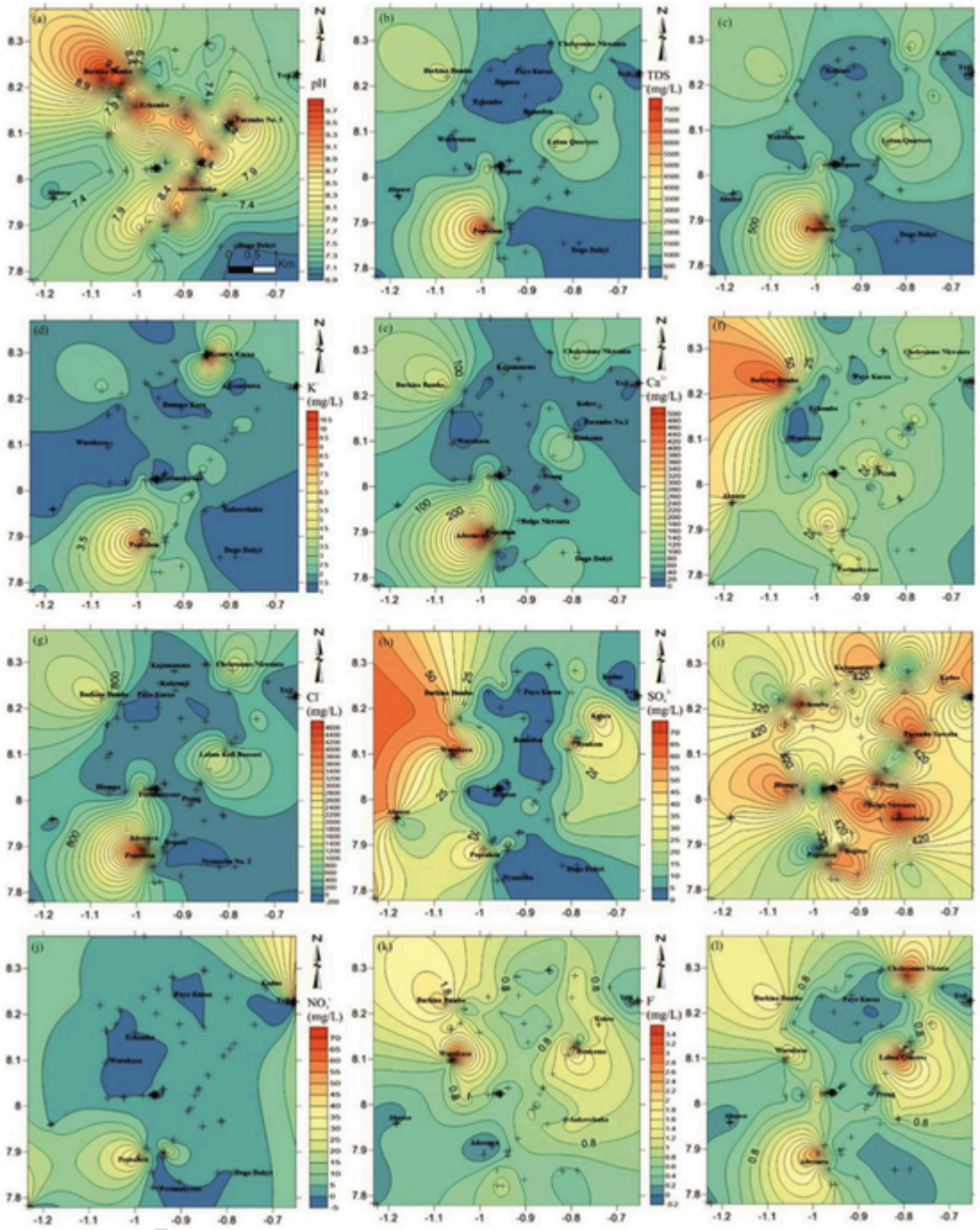

Fig. 5. Spatial distribution maps of the various hydrochemical parameters in groundwater of the semi-arid Pru Basin.

Furthermore, the major ion and chloride relationships still throw more light on the sources of groundwater salinization. The Ca^{2+} versus Cl^- plot (Fig. 10c) indicates that 69% of the samples with higher Ca^{2+} ratios were influenced by mixing of fresh groundwater with saline water (Gopinath et al., 2014). The Mg^{2+} versus Cl^- plot (Fig. 10d) delineates samples influenced by both saline water intrusion (those below the conservative mixing) and weathering of calcium-magnesium minerals in the Oti/Pendjari Group (those above the conservative mixing line) (Gopinath et al., 2018). The relationship between K^+ and Cl^- (Fig. 10e) reveals that samples with high Cl^- ratios might be influenced by ion exchange processes (Gopinath et al., 2018). However, the low K^+ concentration in groundwater may be related with the proclivity of K^+ to be adsorbed by clay minerals to form secondary minerals and agricultural activities in the basin (Gopinath et al., 2018). The B versus Cl^- ratios slightly increased and shifted towards the excess Cl^- field due to possible mixing with saline water from adjacent aquifers (Fig. 10f). The SO_4^{2-} versus Cl^- ratio plot (Fig. 10g) indicates that depletion in SO_4^{2-} is primarily as a result of saline water intrusion (Gopinath et al., 2014). The SO_4^{2-} depletion could also be due to gypsum precipitation in the saline water during the initial stages of intrusion. Majority of the samples show higher values of the SO_4^{2-}/Cl^- and B concentration (Fig. 10h) pointing to evaporate dissolution within the aquifer (Trabelsi et al., 2007). The relationship between TDS and Cl^- (Fig. 10i) indicates an exceptional linear mixing trend with a very strong correlation coefficient ($r = 0.99$). This suggests that

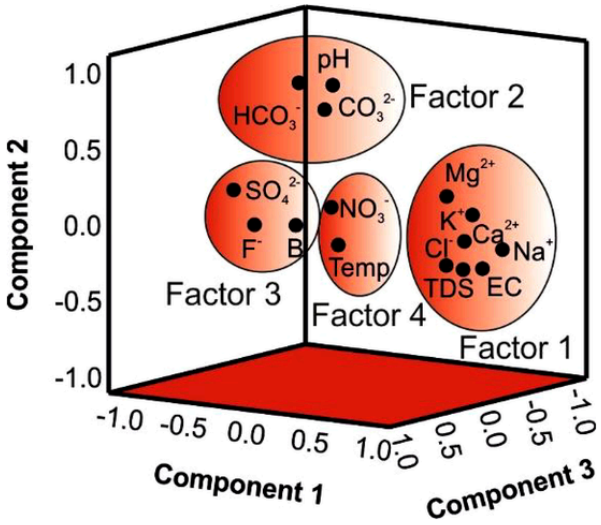

Fig. 6. Rotation plot of R-mode factor analysis showing the ion associations.

Table 5
Saturation indices of the mineral phases in groundwater of the semi-arid Pru Basin (STD = Standard Deviation).

Mineral	Minimum	Maximum	Average	STD.
SI Albite	−5.60	0.27	−2.73	1.15
SI Anhydrite	−6.03	−1.92	−3.35	0.63
SI Aragonite	−0.06	1.22	0.76	0.22
SI Calcite	0.08	1.36	0.90	0.22
SI Chalcedony	−1.24	0.28	−0.47	0.27
SI Dolomite	0.07	2.97	1.79	0.59
SI Fluorite	−2.68	−0.27	−1.81	0.47
SI Gypsum	−5.79	−1.71	−3.14	0.63
SI Halite	−9.01	−3.75	−6.65	0.97
SI Quartz	−0.82	0.75	−0.04	0.28
SI Talc	−4.54	5.54	1.99	1.68

the enrichment of Cl^- in groundwater may be due to saline water mixing processes and the samples with higher TDS might be an indication of water-rock interaction and anthropogenic input (Ebrahimi et al., 2016). In all, it can be inferred from the ionic ratio plots that the source of groundwater salinization in the semi-arid Pru Basin is an interplay of factors comprising saline water intrusion, mixing effects, ion exchange reactions, water-rock interaction and anthropogenic activities. Similar processes are ascribed as the source of groundwater salinization in basins and coastal aquifers with similar climatic conditions in Ghana (Kortatsi, 2007; Egbi et al., 2019), Iran (Ebrahimi et al., 2016), and India (Pratheepa et al., 2015; Karunanidhi et al., 2020).

5.1.4. Anthropogenic activities

The nitrate levels as well as TDS concentration levels are indication of anthropogenic activities in a given area (Sunkari et al., 2019). The nitrate contribution to the chemical content in the groundwater only affects a sample collected from the Yeji Township 2 where the concentration (70.6 mg/L) exceeds the maximum permissible value of 50 mg/L by the WHO (Table 1). However, when all the NO_3^- concentrations are compared with the guideline value (10 mg/L) of the Bureau of Indian Standards (Bureau of Indian Standards, BIS, 2012), the NO_3^- concentrations of hand-dug wells from Nyomoase (33.7 mg/L), Adeemra (43.8 mg/L), Kumfia 1 (33.1), Yeji Catholic Hospital 1 (33.8 mg/L), Yeji Catholic Hospital 2 (33.2 mg/L), and Yeji Township 1 (32.6 mg/L) appear to exceed the threshold. Therefore, approximately 9% of the groundwater resources in the semi-arid Pru Basin are contaminated with nitrates. The affected communities are mostly around the eastern and southwestern parts of the semi-arid Pru Basin where anthropogenic activities such as farming are common. The source of nitrate in groundwater has been traced to the application of nitrate fertilizers (Berhe et al., 2017; Gibrilla et al., 2020). The reasonable positive correlation of NO_3^- with the other ions (Table 3) supports anthropogenic pollution through the continuous application of nitrate fertilizers in farms within the basin. The TDS values are generally higher than the 500 mg/L acceptable level, and anthropogenic activities have proven to be the main source of TDS in groundwater (Berhe et al., 2017; Lermi and Ertan, 2019). On bivariate plots of selected major ions versus TDS, it is observed that about 50% of the groundwater samples are contaminated with respect to higher TDS values with increasing ion concentration (Fig. 11a - d). The increasing trends of Na^+, Mg^{2+}, Cl^-, and NO_3^- with increasing TDS support anthropogenic contribution from agricultural activities, untreated sewage effluents, and household waste leachates (Fig. 11a - d).

5.2. Constraints from multivariate statistical and geochemical modeling approaches

In general, it is difficult to understand geochemical processes due to their complex nature. Applying multivariate statistical techniques to hydrochemical data can show their interrelationships and thus, help decipher their sources (Yidana et al., 2012). In this regard, the results of the R-mode FA give a hint to the sources of the ions in groundwater. The concentrations of EC, TDS, Na^+, K^+, Ca^{2+}, Mg^{2+}, and Cl^- in saline water exceed that of continental freshwater (Trabelsi et al., 2007). Therefore, the association of these parameters with factor 1 (Fig. 6) could be linked to saline water intrusion into the aquifer from adjacent aquifers, which is one of the primary factors controlling the chemistry of groundwater. Also, factor 1 can be associated with water-rock interaction, which dissolved most of the rock constituents and then released these ions into groundwater (Yidana et al., 2012). HCO_3^- and CO_3^{2-} in factor 2 (Fig. 6) are derived from the dissolution of CO_2 in the water and gives a hint on the source of recharge in the basin (Trabelsi et al., 2007). The inclusion of pH in factor 2 (Fig. 6) highlights the significant role it plays in geochemistry of carbonates and clays in the semi-arid Pru Basin. It is therefore associated with carbonate and clay mineral dissolution in the aquifer. Strong positive loading of SO_4^{2-}, F^- and B in factor 3 (Fig. 6) is as a result of ion exchange reactions in the aquifer. However, contribution from anthropogenic activities like application of agrochemicals such as sulphate fertilizers, especially in the southwestern part of the study area may have resulted in this factor loading. Therefore, this factor staggers the boundary between geogenic and anthropogenic sources of the ions. Moreover, temperature and NO_3^- associated with factor 4 (Fig. 6) may be confirming the contribution from anthropogenic sources. Since the surface of the aquifer is used for agricultural activities, the NO_3^- may be derived from surface runoff of nitrate fertilizers.

The saturation of groundwater with respect to calcite and dolomite confirms the dissolution of these minerals from the Kodjari Formation of the Oti/Pendjari Group as explained in the earlier section. On a bivariate plot of SI dolomite versus SI calcite (Fig. 12a), all the studied samples plot in the field of saturation with respect to both minerals. Therefore, the high concentration of Ca^{2+}, Mg^{2+} and HCO_3^- may be as a result of calcite and dolomite dissolution since carbonate weathering is dominant in the study area. The under-saturation of the samples with respect to gypsum (Fig. 12b) and anhydrite suggests that the less concentration of SO_4^{2-} in the groundwater is due to less dissolution of gypsum. The saturation of some of the samples with respect to calcite and aragonite (Fig. 12c) indicates possible dissolution of these minerals in

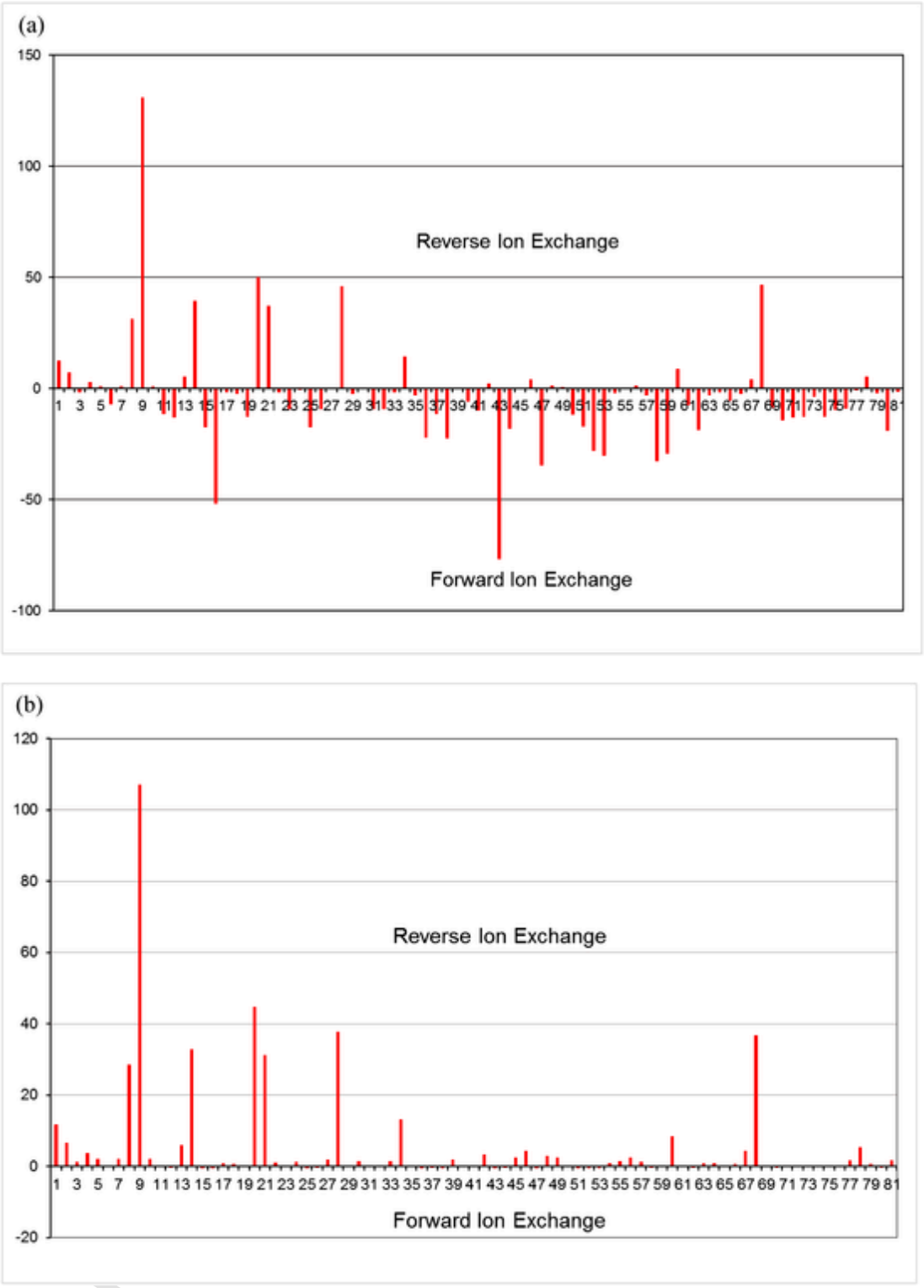

Fig. 7. (a) CAI – 1 and (b) CAI – 2 diagrams showing the extent of forward and reverse ion exchange reactions in the semi-arid Pru Basin.

groundwater. On Fig. 12d, about 85% of the samples plot in the talc saturation zone. Talc occurs as a hydrated magnesium silicate that may be formed from reaction of dolomite and silica or metamorphism of magnesium-bearing minerals in the presence of water and carbon dioxide (Singh et al., 2015). This is consistent with the prevalence of dolomites in the Oti/Pendjari Group. Consequently, saturation of groundwater with respect to talc implies that either processes may be responsible. On the bivariate plot of SI halite versus Cl^- (Fig. 12e), all the samples plot in the halite under-saturation zone implying that halite dissolution can be precluded from influencing the groundwater chemistry. However, the high Cl^- concentration of groundwater can be explained by saline water intrusion and other processes like ion exchange reactions and anthropogenic activities. Fluorite also shows under-saturation in the groundwater (Fig. 12f) but the strong positive

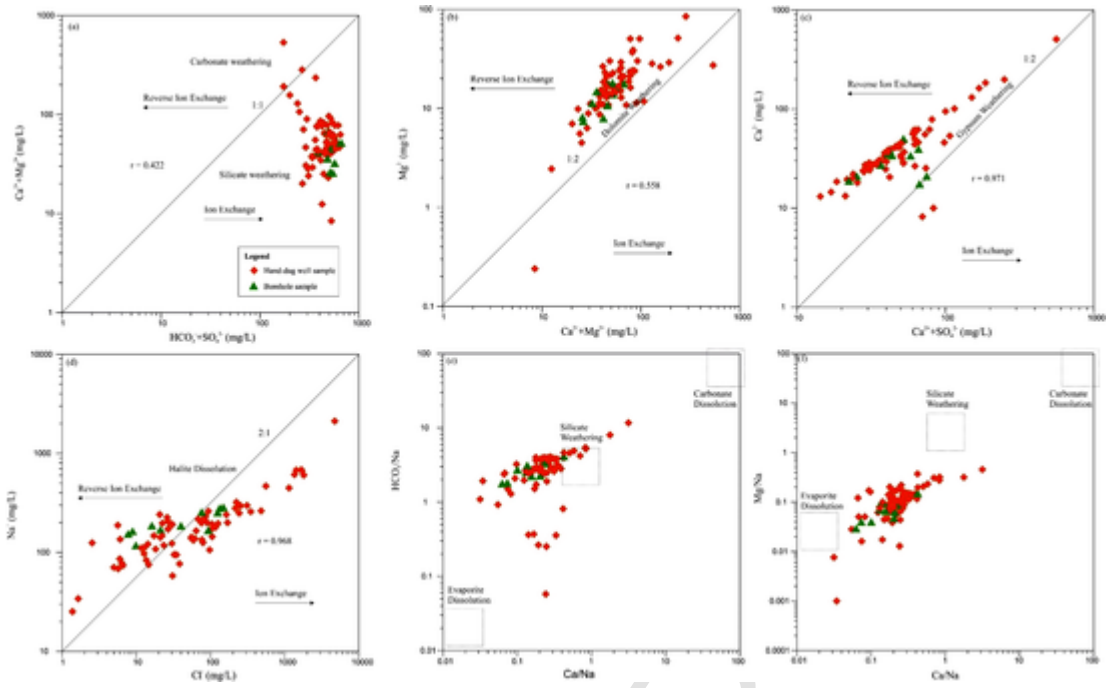

Fig. 8. Molar ratio in bivariate plots of (a) Ca^{2+} + Mg^{2+} versus HCO_3^- + SO_4^{2-}, (b) Mg^{2+} versus Ca^{2+} + Mg^{2+}, (c) Ca^{2+} versus Ca^{2+} + SO_4^{2-}, (d) Na^+ versus Cl^-, (e) Na-normalized Ca versus HCO3, and (d) Na-normalized Ca versus Mg.

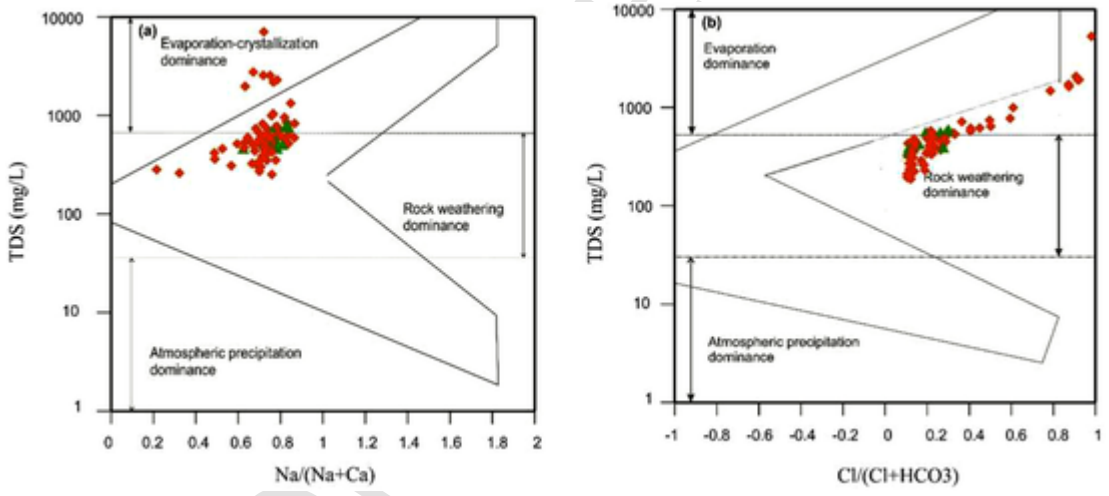

Fig. 9. Gibbs (1970) diagrams showing the controlling factors of groundwater chemistry.

Table 6
Ratios of ion exchange reaction and silicate weathering in the semi-arid Pru Basin.

Parameter	Minimum	Maximum	Average
Na/(Na + Ca)	0.22	0.97	0.79
CAI - 1	−76.8	131	−2.93
CAI - 2	−0.65	107	5.1
Cl/ΣAnions	0.01	0.97	0.24
Mg/(Ca + Mg)	0.05	0.75	0.42
r1	−311	18,982	400
r2	−22,713	10	−335
Na/Cl	0.52	76.4	9.62

correlation of fluorite and F^- may suggest that the F^- enrichment in groundwater of some of the communities reflects the role of Ca^{2+} through ion exchange reaction (Zango et al., 2019). Saturation of some samples with respect to the silicate mineral phases such as albite, chalcedony and quartz (Table 5) explains the role of silicate weathering in groundwater chemistry.

6. Conclusions

Aquifers in semi-arid environments are known to have several hydrogeological complexities and environmental problems. One of them is groundwater salinization and an increase in the concentrations of ions that are detrimental to human health. Also, the use of different ionic ratio plots, multivariate statistical, and geochemical modeling techniques to depict groundwater salinization is still not common in the scientific front. Therefore, this study contributes to the understanding of the vulnerability of semi-arid basin aquifers to long-term salinization in a broad context through the dissolution of groundwater chemical constituents. In this regard, the study has made available new data from the semi-arid Pru Basin in Ghana regarding the geochemical evolution of groundwater from 81 hand-dug wells and boreholes within

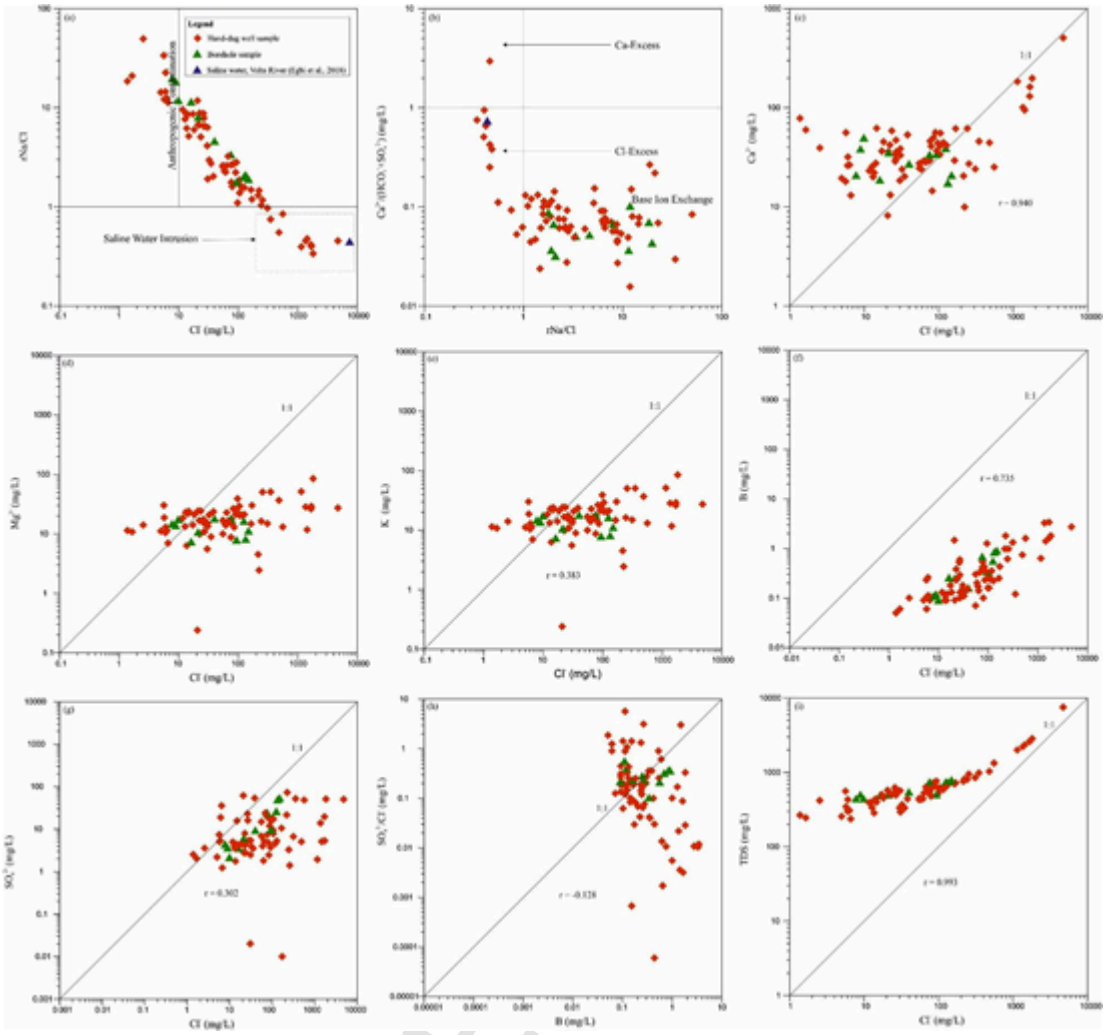

Fig. 10. Sources of groundwater salinization from bivariate plots of (a) rNa/Cl versus Cl-, (b) Ca/(HCO3 + SO4) versus rNa/Cl, (c) Ca^{2+} versus Cl^{-}, (d) Mg^{2+} versus Cl^{-}, (e) K^{+} versus Cl^{-}, (f) B versus Cl^{-}, (g) SO_4^{2-} versus Cl^{-}, (h) SO_4^{2-}/Cl^{-}, and (i) TDS versus Cl^{-}.

the siliciclastic Pru Formation of the Oti/Pendjari Group in the basin. It is the first to document evidence of groundwater salinization in the semi-arid Pru Basin using an integrated approach involving different ionic ratio plots, multivariate statistical analyses, and geochemical modeling. The findings of the study revealed that:

- The abundance of major ions follows the order: $Na^{+} > Ca^{2+} > Mg^{2+} > K^{+}$ and $Cl^{-} > HCO_3^{-} > SO_4^{2-}$.
- Groundwater in the semi-arid Pru Basin evolved from a less saline Na-HCO3, Na-Ca-HCO3 and Na-Mg-HCO3 water type to a more saline Na-HCO3-Cl water type.
- The main controls of groundwater chemistry are water – rock interaction, ion exchange reactions, silicate and carbonate weathering, salinization and anthropogenic activities like application of agrochemicals to farms and shallow meteoric water infiltration from agricultural lands.
- The ionic ratio plots (involving Na^{+}, K^{+}, Ca^{2+}, Mg^{2+}, Cl^{-}, SO_4^{2-} and B) and multivariate statistical analyses indicate that groundwater salinization is as a result of geogenic processes and anthropogenic activities.
- Revelle index indicated that the groundwater salinization affected about 19.8% of the studied samples: the southwestern part of the basin is the most affected.
- Mineral saturation indices calculated using PHREEQC demonstrate that groundwater is generally saturated with respect to carbonate minerals (calcite, aragonite, talc) and silicate minerals (albite, chalcedony, quartz) but under-saturated with respect to anhydrite, fluorite, gypsum, and halite.
- It is recommended that to mitigate the threat of groundwater salinization, the basin water level should be kept high, artificial subsurface barriers should be developed, rainwater harvesting technology should be used, artificial recharge structures should be adopted and aquifer improvement plans should be implemented.
- Future researches in the area should focus on using isotopes to completely understand the source of groundwater salinization.

CRediT authorship contribution statement

Emmanuel Daanoba Sunkari: Conceptualization, Methodology, Software, Formal analysis, Writing - original draft, Writing - review & editing. **Mahamuda Abu:** Visualization, Data curation, Validation, Writing - original draft. **Musah Saeed Zango:** Funding acquisition, Resources, Investigation, Supervision.

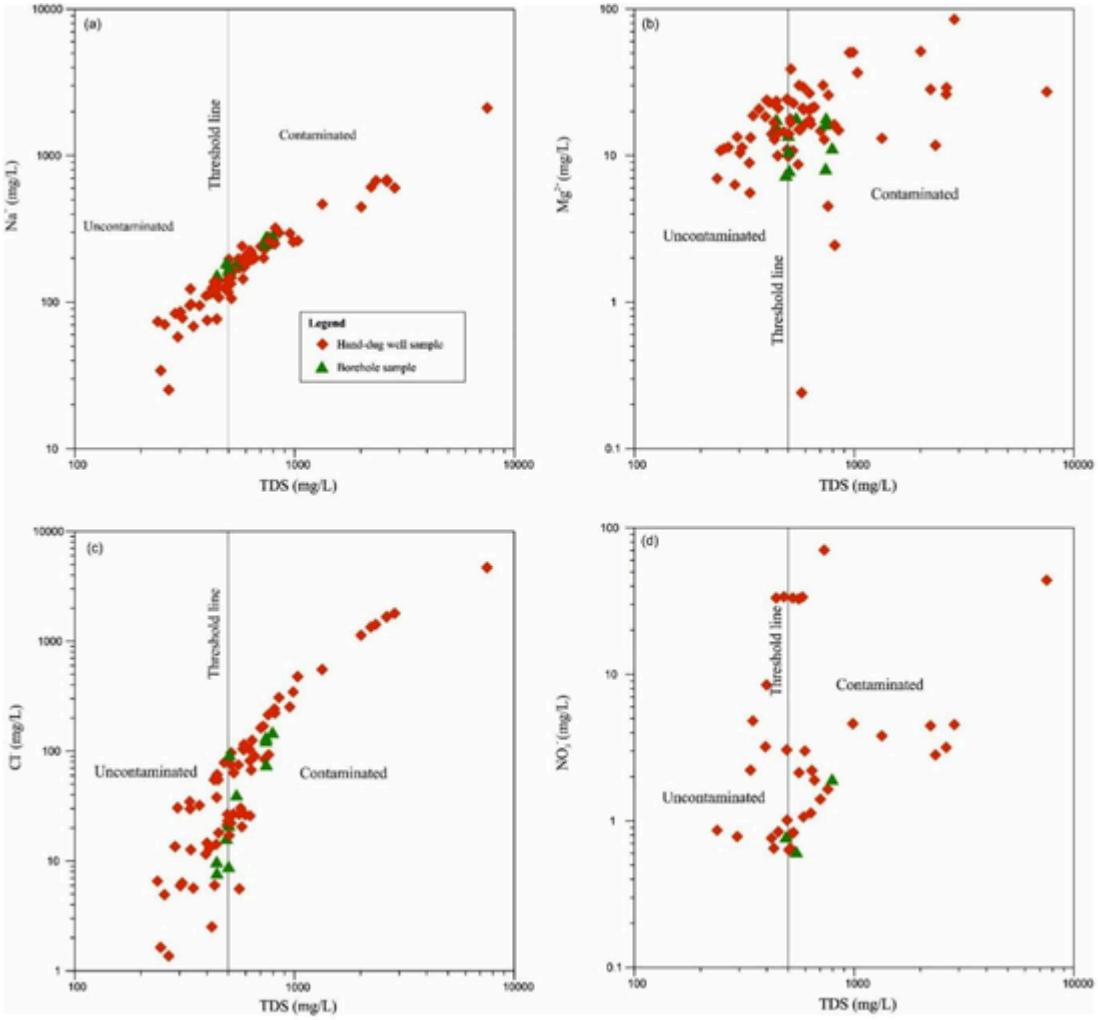

Fig. 11. Relationship between major ions and TDS showing some level of anthropogenic pollution of the groundwater.

Declaration of Competing Interest

The authors declare that they have no known competing financial interests or personal relationships that could have appeared to influence the work reported in this paper.

Acknowledgement

The first author thanks BIDEB 2215 Graduate Scholarship Program of the Scientific and Technological Research Council of Turkey (TÜBİTAK) for the continuous support as a doctoral research fellow. The second and third authors acknowledge Earth Science department of the Faculty of Earth and Environmental Sciences, CK Tedam University of Technology and Applied Sciences, Ghana for logistic support during the field studies and water sample collection. The Government of Ghana's annual research fund support to faculty members is also acknowledged. The Editor and Reviewers are thanked for the valuable comments that improved the quality of this paper.

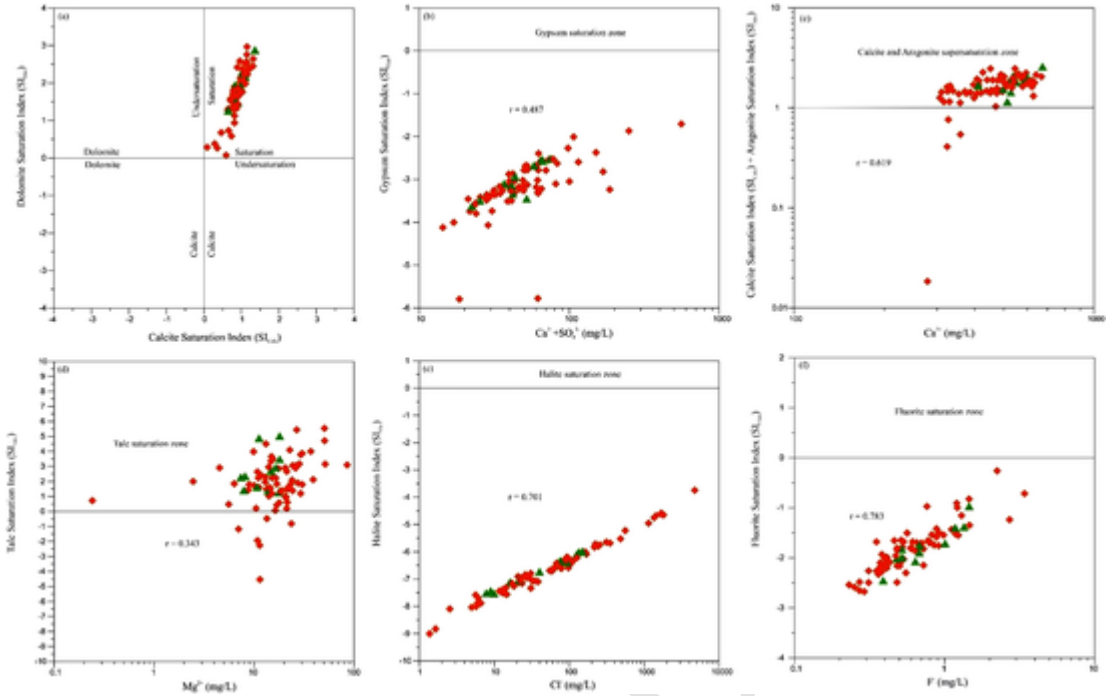

Fig. 12. Bivariate plots of saturation indices and major ions (a) SI Dolomite versus SI Calcite, (b) SI Gypsum versus Ca^{2+} + SO_4^{2-}, (c) SI Calcite + SI Aragonite versus Ca^{2+}, (d) SI Talc versus Mg^{2+}, (e) SI Halite versus Cl^{-}, and (f) SI Fluorite versus F^{-}.

References

Abanyie, S.K., Sunkari, E.D., Apea, O.B., Abagale, S., Korboe, H.M., 2020. Assessment of the quality of water resources in the Upper East Region, Ghana: a review. Sustai. Water Resourc. Manag. 6, 52. doi:10.1007/s40899-020-00409-4.

Abdalla, F., 2016. Ionic ratios as tracers to assess seawater intrusion and to identify salinity sources in Jazan coastal aquifer, Saudi Arabia. Arab. J. Geosci. 9 (1), 40. doi:10.1007/s12517-015-2065-3.

Abu, M., Sunkari, E.D., Şener, M., 2019. Untapped economic resource potential of the neoproterozoic to early Paleozoic Volta Basin, Ghana: a review. Nat. Resour. Res. 28, 1429–1445. doi:10.1007/s11053-019-09478-5.

Affaton, P., 2008. Lithostratigraphy of the Volta basin and related structural units. In The Voltaian Basin, Ghana. Workshop and Excursion, pp. 13–17.

Ako, A.A., Shimada, J., Hosono, T., Kagabu, M., Ayuk, A.R., Nkeng, G.E., Takounjou, A.L.F., 2012. Spring water quality and usability in the Mount Cameroon area revealed by hydrogeochemistry. Environ. Geochem. Health 34 (5), 615–639.

Ammar, S.B., Taupin, J.D., Alaya, M.B., Zouari, K., Patris, N., Khouatmia, M., 2020. Using geochemical and isotopic tracers to characterize groundwater dynamics and salinity sources in the Wadi Guenniche coastal plain in northern Tunisia. J. Arid Environ. 178, 104150. doi:10.1016/j.jaridenv.2020.104150.

Belkhiri, L., Boudoukha, A., Mouni, L., Baouz, T., 2010. Application of multivariate statistical methods and inverse geochemical modeling for characterization of groundwater—a case study: Ain Azel plain (Algeria). Geoderma 159 (3–4), 390–398.

Belkhiri, L., Mouni, L., Boudoukha, A., 2012. Geochemical evolution of groundwater in an alluvial aquifer: case of El Eulma aquifer, East Algeria. J. Afr. Earth Sci. 66, 46–55.

Berhe, B.A., Dokuz, U.E., Celik, M., 2017. Assessment of hydrogeochemistry and environmental isotopes of surface and groundwaters in the Kutahya Plain, Turkey. J. Afr. Earth Sci. 134, 230–240.

Borrok, D.M., Engle, M.A., 2014. The role of climate in increasing salt loads in dryland rivers. J. Arid Environ. 111, 7–13. doi:10.1016/j.jaridenv.2014.07.001.

Bureau of Indian Standards, BIS, 2012. IS:10500 Indian Standard for Drinking Water Specification. In: Second Revision. India, New Delhi.

Busico, G., Cuoco, E., Kazakis, N., Colombani, N., Mastrocicco, M., Tedesco, D., Voudouris, K., 2018. Multivariate statistical analysis to characterize/discriminate between anthropogenic and geogenic trace elements occurrence in the campania plain, southern italy. Environ. Pollut. 234, 260–269. doi:10.1016/j.envpol.2017.11.053.

Carney, J., Jordan, C., Thomas, C., McDonnell, P., 2008. A revised lithostratigraphy and geological map for the Volta Basin, derived from image interpretation and field mapping.

Cartwright, I., Morgenstern, U., 2012. Constraining the groundwater recharge and the rate of geochemical processes using tritium and major ion geochemistry: ovens catchment, southeast Australia. J. Hydrol. 475, 137–149.

Chegbeleh, L.P., Akurugu, B.A., Yidana, S.M., 2020. Assessment of Groundwater Quality in the Talensi District, Northern Ghana. Sci. World J. 2020. doi:10.1155/2020/8450860.

Çiner, F., Sunkari, E.D., Şenbaş, B.A., 2020. Geochemical and Multivariate Statistical Evaluation of Trace Elements in Groundwater of Niğde Municipality, South-Central Turkey: Implications for Arsenic Contamination and Human Health Risks Assessment. Arch. Environ. Contam. Toxicol. 1–19. doi:10.1007/s00244-020-00759-2.

Dapaah-Siakwan, S., Gyau-Boakye, P., 2000. Hydrogeologic framework and borehole yields in Ghana. Hydrogeol. J. 8 (4), 405–416.

Ebrahimi, M., Kazemi, H., Ehtashemi, M., Rockaway, T.D., 2016. Assessment of groundwater quantity and quality and saltwater intrusion in the Damghan basin, Iran. Geochemistry 76 (2), 227–241.

Emenike, P.C., Nnaji, C.C., Tenebe, I.T., Agunwamba, J.C., 2020. Hydrogeochemical imprints and spatio-temporal health risk assessment of lead in drinking water sources of Abeokuta, south-western Nigeria. Int. J. Environ. Sci. Technol. 17 (1), 343–360. doi:10.1007/s13762-019-02506-0.

Gaillardet, J., Dupre, B., Louvat, P., Allegre, C.J., 1999. Global silicate weathering and CO2 consumption rates deduced from the chemistry of large rivers. Chem. Geol. 159, 3–30.

Gibbs, R.J., 1970. Mechanisms controlling world water chemistry. Science 17, 1088–1090. doi:10.1126/science.170.3962.1088.

Gibrilla, A., Fianko, J.R., Ganyaglo, S., Adomako, D., Anornu, G., Zakaria, N., 2020. Nitrate contamination and source apportionment in surface and groundwater in Ghana using dual isotopes (15N and 18O-NO3) and a Bayesian isotope mixing model. J. Contam. Hydrol. 103658. doi:10.1016/j.jconhyd.2020.103658.

Gnanachandrasamy, G., Ramkumar, T., Venkatramanan, S., Vasudevan, S., Chung, S.Y., Bagyaraj, M., 2015. Accessing groundwater quality in lower part of Nagapattinam district, Southern India: using hydrogeochemistry and GIS interpolation techniques. Appl Water Sci 5 (1), 39–55.

Gopinath, S., Srinivasamoorthy, K., Prakash, R., 2014. Hydrochemical investigations for identification of groundwater salinization sources in Nagapattinam and Karaikal regions, Southern India. Environ GeoChim Acta 1 (2), 153–160.

Gopinath, S., Srinivasamoorthy, K., Vasanthavigar, M., Saravanan, K., Prakash, R., Suma, C.S., Senthilnathan, D., 2018. Hydrochemical characteristics and salinity of groundwater in parts of Nagapattinam district of Tamil Nadu and the Union Territory of Puducherry, India. Carbonates Evaporites 33 (1), 1–13.

Griffis, R.J., Barning, K., Agezo, F.L., Akosah, F.K., 2002. Gold deposits of Ghana. Minerals Commission, Accra, Ghana 432.

Junner, N.R., Hirdes, T., 1946. The geology and hydrology of the Voltaian Basin. Memoir 8. Accra: Gold Coast Geological Survey 8, 51.

Karunanidhi, D., Aravinthasamy, P., Deepali, M., Subramani, T., Sunkari, E.D., 2020. Appraisal of subsurface hydrogeochemical processes in a geologically heterogeneous semi-arid region of south India based on mass transfer and fuzzy comprehensive modeling. Environ. Geochem. Health 1–20. doi:10.1007/s10653-020-00676-2.

Kass, A., Gavrieli, I., Yechieli, Y., Vengosh, A., Starinsky, A., 2005. The impact of freshwater and wastewater irrigation on the chemistry of shallow groundwater: a case study from the Israeli Coastal Aquifer. J. Hydrol. 300 (1–4), 314–331.

Kaur, L., Rishi, M.S., Sharma, S., Sharma, B., Lata, R., Singh, G., 2019. Hydrogeochemical characterization of groundwater in alluvial plains of River Yamuna in Northern India: an insight of controlling processes. J. King Saud Univ.-Sci. 31 (4), 1245–1253.

Keesari, T., Dauji, S., 2020. Groundwater salinization processes: pitfalls of inferences from Na+/Cl− versus Cl− correlation plots. Environ. Geochem. Health. doi:10.1007/s10653-020-00622-2.

Kortatsi, B.K., 2007. Hydrochemical framework of groundwater in the Ankobra Basin, Ghana. Aquat. Geochem. 13 (1), 41–74.

Kumar, M., Ramanathan, A.L., Ranjan, S., Singh, V.B., Kumar, N., Yadav, S.K., Rao, M.S., Ritch, S., Bhattacharya, P., 2018. Groundwater evolution and its utility in upper Ganges-Yamuna Alluvial plain of Northern India, India: Evidence from solute chemistry and stable isotopes. Groundw. Sustain. Dev. 7, 400–409.

Lermi, A., Ertan, G., 2019. Hydrochemical and isotopic studies to understand quality problems in groundwater of the Niğde Province, Central Turkey. Environ. Earth Sci. 78 (12), 365. doi:10.1007/s12665-019-8365-2.

Li, P., Wu, J., Qian, H., 2016. Hydrochemical appraisal of groundwater quality for drinking and irrigation purposes and the major influencing factors: a case study in and around Hua County. China. Arabian J. Geosci. 9 (1), 15. doi:10.1007/s12517-0152059-1.

Loh, Y.S.A., Akurugu, B.A., Manu, E., Abdul-Samed, A., 2019. Assessment of groundwater quality and the main controls on its hydrochemistry in some Voltaian and basement aquifers, northern Ghana, Groundwater for Sustainable Development (2019). doi:10.1016/j.gsd.2019.100296.

Lyons, W.B., Welch, S.A., Gardner, C.B., Sharifi, A., AghaKouchak, A., Mashkour, M., Djamali, M., Matinzadeh, Z., Palacio, S., Akhani, H., 2020. The hydrogeochemistry of shallow groundwater from Lut Desert, Iran: The hottest place on Earth. J. Arid Environ. 178, 104143. doi:10.1016/j.jaridenv.2020.104143.

Matthes, G., 1982. The Properties of Groundwater. John Wiley and Sons, New York, 406. In: ISBN0–471–08513-8.

McLean, W., Jankowski, J., 2000. Groundwater quality and sustainability in an alluvial aquifer, Australia. In: Sililo, et al. (Ed.), Proc. XXX IAH congress on Groundwater: Past Achievements and Future Challenges. Cape Town South Africa 26th November–1st December 2000. AA Balkema, Rotterdam, Brookfield.

Moghaddam, A.A., Fijani, E., 2008. Distribution of fluoride in groundwater of Maku area, northwest of Iran. Environ. Geol. 56 (2), 281–287.

Naily, W., 2018. February. Ratio of Major Ions in Groundwater to Determine Saltwater Intrusion in Coastal Areas. In: IOP Conference Series: Earth and Environmental Science. 118(1), 012021. IOP Publishing.

Najib, S., Fadili, A., Mehdi, K., Riss, J., Makan, A., 2017. Contribution of hydrochemical and geoelectrical approaches to investigate salinization process and seawater intrusion in the coastal aquifers of Chaouia, Morocco. J. Contam. Hydrol. 198, 24–36.

Naseem, S., Rafique, T., Bashir, E., Bhanger, M.I., Laghari, A., Usmani, T.H., 2010. Lithological influences on occurrence of high-fluoride groundwater in Nagar Parkar area, Thar Desert, Pakistan. Chemosphere 78 (11), 1313–1321.

Parkhurst, D.L., Appelo, C.A.J., 1999. User's guide to PHREEQC (Version 2): a computer program for speciation, batch-reaction, one-dimensional transport, and inverse geochemical calculations. Water Res Invest Rep 99 (4259), 312.

Piper, A.M., 1953. A graphic representation in the geochemical interpretation of groundwater analyses. Am. Geophys. Union Trans. USA 25, 914–923.

Pratheepa, V., Ramesh, S., Sukumaran, N., Murugesan, A.G., 2015. Identification of the sources for groundwater salinization in the coastal aquifers of Southern Tamil Nadu, India. Environ. Earth Sci. 74 (4), 2819–2829.

Rufino, F., Busico, G., Cuoco, E., Darrah, T.H., Tedesco, D., 2019. Evaluating the suitability of urban groundwater resources for drinking water and irrigation purposes: An integrated approach in the agro-aversano area of southern Italy. Environ. Monit. Assess. 191 (12), 768. doi:10.1007/s10661-019-7978-y.

Salifu, A., Petrusevski, B., Ghebremichael, K., Buamah, R., Amy, G., 2012. Multivariate statistical analysis for fluoride occurrence in groundwater in the Northern region of Ghana. J. Contam. Hydrol. 140, 34–44.

Schoeller, H., 1965. Qualitative evaluation of groundwater resources. In: Methods and techniques of groundwater investigations and development. UNESCO, pp. 54–83.

Sikah, J.N., Aning, A.A., Danuor, S.K., Manu, E., Okrah, C., 2016. Groundwater Exploration using 1D and 2D Electrical Resistivity Methods. J. Environ. Earth Sci. 6 (7), 55–63.

Singh, N., Singh, R.P., Kamal, V., Sen, R., Mukherjee, S., 2015. Assessment of hydrogeochemistry and the quality of groundwater in 24-Parganas districts, West Bengal. Environ. Earth Sci. 73 (1), 375–386.

Song, S.H., Lee, J.Y., Park, N., 2007. Use of vertical electrical soundings to delineate seawater intrusion in a coastal area of Byunsan, Korea. Environ. Geol. 52 (6), 1207–1219.

Stuyfzand, P.J., 1999. Patterns in groundwater chemistry resulting from groundwater flow. Hydrogeol. J. 7 (1), 15–27. doi:10.1007/s100400050177.

Sunkari, E.D., Abu, M., 2019. Hydrochemistry with special reference to fluoride contamination in groundwater of the Bongo district, Upper East Region, Ghana. Sustai. Water Resourc. Manag. 5 (4), 1803–1814. doi:10.1007/s40899-019-00335-0.

Sunkari, E.D., Zango, M.S., Korboe, H.M., 2018. Comparative analysis of fluoride concentrations in groundwaters in northern and southern Ghana: implications for the contaminant sources. Earth Syst. Environ. 2 (1), 103–117. doi:10.1007/s41748-018-0044-z.

Sunkari, E.D., Abu, M., Bayowobie, P.S., Dokuz, U.E., 2019. Hydrogeochemical appraisal of groundwater quality in the Ga west municipality, Ghana: Implication for domestic and irrigation purposes. Groundw. Sustain. Dev. 8, 501–511. doi:10.1016/j.gsd.2019.02.002.

Sunkari, E.D., Abu, M., Zango, M.S., Wani, A.M.L., 2020. Hydrogeochemical characterization and assessment of groundwater quality in the Kwahu-Bombouaka Group of the Voltaian Supergroup, Ghana. J. Afr. Earth Sci. 103899. doi:10.1016/j.jafrearsci.2020.103899.

Trabelsi, R., Zairi, M., Dhia, H.B., 2007. Groundwater salinization of the Sfax superficial aquifer, Tunisia. Hydrogeol. J. 15 (7), 1341–1355.

World Health Organization, W.H.O, 2017. Guidelines for drinking-water quality: fourth edition incorporating the first addendum. WHO, Geneva.

Yidana, S.M., Banoeng-Yakubo, B., Aliou, A.S., Akabzaa, T., 2012. Groundwater quality in some Voltaian and Birimian aquifers in northern Ghana—application of mulitvariate statistical methods and geographic information systems. Hydrol. Sci. J. 57 (6), 1168–1183.

Yidana, S.M., Bawoyobie, P., Sakyi, P., Fynn, O.F., 2018. Evolutionary analysis of groundwater flow: Application of multivariate statistical analysis to hydrochemical data in the Densu Basin, Ghana. J. Afr. Earth Sci. 138, 167–176.

Zango, M.S., Sunkari, E.D., Abu, M., Lermi, A., 2019. Hydrogeochemical controls and human health risk assessment of groundwater fluoride and boron in the semi-arid North East region of Ghana. J. Geochem. Explor. 207, 106363. doi:10.1016/j.gexplo.2019.106363.